Title

Probing neurophysiological function in the outer retina using chemogenetic manipulation and optogenetic sensors

Author

Beckwith-Cohen, Billie

Publication Date

2021

Peer reviewed|Thesis/dissertation

Probing neurophysiological function in the outer retina using chemogenetic manipulation and optogenetic sensors

By

Billie Beckwith-Cohen

A dissertation submitted in partial satisfaction of the

requirements for the degree of

Doctor of Philosophy

in

Vision Science

in the

Graduate Division
of the

University of California, Berkeley

Committee in charge:
Professor Richard H. Kramer, Chair
Professor Marla B. Feller
Professor Stephen G. Brohawn
Spring 2021

Abstract

Probing neurophysiological function in the outer retina
using chemogenetic manipulation and optogenetic sensors

by

Billie Beckwith-Cohen

Doctor of Philosophy in Vision Science

University of California, Berkeley

Richard H. Kramer, Chair

The retina offers unique insight into synaptic activity in the central nervous system. It is the only part of the central nervous system that can be visualized without advanced imaging or invasive methods. Its highly organized structure has turned it into a main target for neuroscientific studies, and while it has a simplistic anatomical organization its synaptic functions have only been partially elucidated. Zebrafish have been utilized to study vision since they have a cone-rich retina, high acuity vision and they are a convenient model to work with and manipulate genetically. Furthermore, zebrafish can absorb drugs and small molecules directly from their liquid environment thereby facilitating chemical manipulation of their nervous system. For these reasons we have chosen to use zebrafish to generate tools that improve our understanding of retinal synaptic activity in the outer plexiform layer of the retina, and in horizontal cells (HCs) in particular. Five genetically modified strains of zebrafish (4 of which were developed at the Kramer lab) are presented in this dissertation. Two strains have been modified using the introduction of foreign receptors, FaNaC and PSAM-GlyR, allowing controlled and reversible depolarization and hyperpolarization of HCs, respectively. Using these modified strains, we show that by changing the membrane potential of HCs we can manipulate neuronal function upstream, and downstream to the HC synapse. Using three additional strains, we explore the change in pH at different locations in the HC to cone synapse during lateral inhibition. Those locations include the AMPA receptor on HCs, and synaptophysin and the voltage gated calcium channel on the photoreceptor side. By combining our chemogenic tool FaNaC to depolarize HCs, and a genetically introduced pHluorin to detect pH changes, we reaffirm the hypothesis that pH is the signal which mediates lateral inhibition in the outer retina. Using the three pH probes, we show that the change in pH is highly localized nearby photoreceptor voltage-gated calcium channels. In conclusion, while HCs form a wide interconnected network that spans the entire retina, their communication with individual photoreceptors through acidification of the synaptic cleft is spatially constrained. Moreover, slight deviations in HC membrane potential greatly alter their effects on other retinal neurons including photoreceptors, bipolar cells, and retinal ganglion cells.

Table of contents

I dedicate this thesis to my beloved brothers, Adam and Maxim.

Acknowledgments

This work would have not been possible without the contributions of many talented and kind individuals on Campus and particularly, within the department of Vision Science. I would like to thank Prof. Richard Kramer, my mentor, for his intellectual, scientific and logistical support during the years of my program; Prof. John Flanagan, Dean of Optometry for his professional and emotional support. Additionally, I would like to thank Profs. John Flannery, Marla Feller and Alexandre Tiriac of the Feller lab, Stephen Brohawn, Paul Malchow and Scott Nawy; my colleagues at the Kramer lab, the ASAO of Optometry, and my fellow Vision Science Graduate Students. Mostly I would like to thank my family, who has been patient and supportive throughout my studies, particularly my mother Carol, my partner Shane, and my sons Bear and Torin.

Chapter 1: Introduction

The vertebrate retina has three main layers of neurons, starting with photoreceptors which sense light, and transmit its signal downstream through bipolar cells to the ganglion cells of the inner retina, and onward to the brain (Wässle 2004). The two main types of retinal photoreceptors, rods and cones, are able to absorb a so-called analog signal in the form of photons of light, and convert it into an electrical gradient, or digital signal, which generates a cascade of intricate retinal responses (Baden et al., 2013). Those responses propagate upstream in the retina and are subject to an array of sign conserving and sign inverting synapses. Cones will transmit their signals to 11 known types of ON- and OFF-bipolar cells, and rods communicate via the ON bipolar cell pathway (Euler et al., 2014). The retinal circuit is even more elaborate as these signals are communicated to an estimated 36 types of retinal ganglion cells (Baden et al., 2016). Retinal communication is modified by a network of interneurons including horizontal cells, amacrine cells, inhibitory and excitatory synapses, as well as direct cellular communication via hemichannels.

The complex interpretation of color, contrast and movement is made possible by the large array of neurons and interneurons described above. The interneurons serve to modify the communications of the 3 primary retinal neurons: photoreceptors, bipolar cells and ganglion cells (Masland 2001). Perhaps the most prominent interneurons that modify the response to light are amacrine cells and horizontal cells (HCs). The latter will be the focus of this dissertation. Horizontal cells are laterally projecting interneurons that share reciprocal synaptic connections with photoreceptors and act upon them through both positive and negative feedback mechanisms. There are an estimated 3 types of HCs in most vertebrate retinae, each of those forms a network with HCs of the same type, which span the entire retina in a mosaic of cells (Hoon et al., 2014). When injecting a dye into one of these HCs, the entire network will obtain the dye since the HCs are interconnected via gap junctions and hemichannels. In the outer plexiform layer of the retina, HCs form a synaptic triad with photoreceptors and bipolar cells. This arrangement establishes the antagonistic center/surround receptive field properties of downstream neurons.

Although HC-mediated lateral inhibition was discovered over half a century ago, its underlying synaptic mechanisms are only partially understood and continue to be the focus of research. Several theories have been proposed with regards to the signal transmitted from HCs to photoreceptors (Kramer and Davenport, 2015). Popular theories as to the signal that mediates lateral inhibition have includes the inhibitory neurotransmitter GABA (Barnes et al., 2020), an ephaptic signal (which relies on a change in current mediated by connexin hemichannels) (Kamermans et al., 2001) and more recently a proton mediated signal (Wang et al., 2014). According to the pH theory, light which hyperpolarizes HCs drives an alkalinization of the synaptic cleft (Wang et al., 2014). Depolarization of the HC, either in the dark or via use of exogenous receptors introduced to the cell will cause an acidification of the synaptic cleft (Wang et al., 2014). Prior studies have shown that lateral inhibition is disrupted if alkalinization of the cleft is prevented, either via the use of the buffer HEPES, or by exogenously inducing HC depolarization (Wang et al., 2014).

The reciprocal synapse between HCs and photoreceptors is anatomically small and invaginated and has thus complicated selective manipulation of HCs alone making them difficult to study via direct manipulation (e.g. patch clamping) (Kramer and Davenport, 2015). This dissertation presents tools intended to facilitate the study of the complex HC-photoreceptor synapse and furthers our knowledge regarding the effects that HCs induce on their synaptic environment and on neurons upstream and downstream in the retina.

Chapter 2 describes methods for exclusive, direct, and reversible manipulation of HC membrane potential. After establishing transgenic chemogenetic methods to hyperpolarize and depolarize HCs, we explored the effects of such manipulations on sequential retinal function. In Chapter 4, I describe experiments in which we integrate our ability to selectively depolarize horizontal cells with a probe to sense pH changes in the synaptic cleft. Further, we utilize three probes to sense changes in pH in various locations of the invaginated HC-photoreceptor synapse to localize the pH signal that underlies feedback inhibition. We conclude that manipulating the membrane potential of HCs can suppress light-induced feedback, affecting the activity of photoreceptors, bipolar cells, and center/surround in ganglion cells. Additionally, we uncover that the pH-signal from HCs to photoreceptors is highly localized nearby the voltage-gated calcium channel on photoreceptor pedicles.

Chapter 2: Controlling horizontal cell-mediated lateral inhibition in transgenic zebrafish retina with chemogenetic tools

Published in the Journal eNeuro in October 2020

Billie Beckwith-Cohen[1], Lars C. Holzhausen[2], Scott Nawy[2] and Richard H. Kramer[1,2]

[1]Vision Science Graduate Program, University of California, Berkeley, School of Optometry, 524 Minor Ln, Berkeley, CA 94720

[1,2]Department of Molecular and Cell Biology, University of California, Berkeley, Life Sciences Addition, #3200, Berkeley, CA 94720

Funding sources:

This work was supported by the National Institutes of Health (grant numbers R01 EY024334 and P30 EY003176).

Citation:

Beckwith-Cohen B, Holzhausen LC, Nawy S, Kramer RH. Controlling Horizontal Cell-Mediated Lateral Inhibition in Transgenic Zebrafish Retina with Chemogenetic Tools. eNeuro. 2020 Oct 26;7(5):ENEURO.0022-20.2020. doi: 10.1523/ENEURO.0022-20.2020. PMID: 33060180; PMCID: PMC7665903.

ABSTRACT

Horizontal Cells (HCs) form reciprocal synapses with rod and cone photoreceptors, an arrangement that underlies lateral inhibition in the retina. HCs send negative and positive feedback signals to photoreceptors, but how HCs initiate these signals remains unclear. Unfortunately, because HCs have no unique neurotransmitter receptors, there are no pharmacological treatments for perturbing membrane potential specifically in HCs. Here we utilize transgenic zebrafish whose HCs express alien receptors, enabling cell-type specific control by cognate alien agonists. To depolarize HCs, we used the FMRFamide-gated Na^+ channel (FaNaC) activated by the invertebrate neuropeptide FMRFamide. To hyperpolarize HCs we used PSAM-GlyR, an engineered Cl^--selective channel activated by a synthetic agonist. Expression of FaNaC or PSAM-GlyR was restricted to HCs with the cell-type selective promoter for connexin-55.5. We assessed HC-feedback control of photoreceptor synapses in three ways. First, we measured presynaptic exocytosis from photoreceptor terminals using the fluorescent dye FM1-43. Second, we measured the electroretinogram (ERG) b-wave, a signal generated by postsynaptic responses. Third, we used Ca^{2+} imaging in retinal ganglion cells (RGCs) expressing the Ca^{2+} indicator GCaMP6. Addition of FMRFamide significantly decreased FM1-43 destaining in darkness, whereas the addition of PSAM-GlyR significantly increased it. However, both agonists decreased the light-elicited ERG b-wave and eliminated surround inhibition of the Ca^{2+} response of RGCs. Taken together, our findings show that chemogenetic tools can selectively manipulate negative feedback from HCs, providing a platform for understanding its mechanism and helping to elucidate its functional roles in visual information processing at a succession of downstream stages.

SIGNIFICANCE STATEMENT

Horizontal cells (HCs) are laterally projecting interneurons that share reciprocal synaptic connections with photoreceptors, an arrangement that establishes the antagonistic center/surround receptive field properties of downstream neurons in the retina and onward into the brain. HC-mediated lateral inhibition was discovered over half a century ago, yet its underlying synaptic mechanisms remain incompletely understood. This is largely because the reciprocal synapse complicates selective manipulation of HCs alone. Here, we utilize chemogenetic tools to bypass photoreceptors and directly manipulate HC membrane potential to reveal feedback effects on sequential steps in synaptic processing of visual information.

INTRODUCTION

Lateral inhibition in the vertebrate retina depends on reciprocal synaptic communication between rod or cone photoreceptors and horizontal cells (HCs) (Thoreson and Mangel, 2012; Kramer and Davenport, 2015). Photoreceptors have a sign-preserving excitatory synapse onto HCs, and HCs exert wide-field sign-inverting negative feedback and narrow-field positive feedback back onto the photoreceptors (Baylor et al., 1971; Jackman et al., 2011). The net effect of HC feedback is that bipolar cells, which carry the light response from the outer to the inner retina, exhibit an antagonistic center-surround receptive field, a property critical for enhancing contrast sensitivity in the visual system and enabling high-acuity vision. In cold-blooded vertebrates, HC feedback also plays critical roles in light adaptation and color information processing (Thoreson and Mangel, 2012). Despite decades of study, the mechanisms underlying HC feedback onto photoreceptors are still being unraveled, largely because the reciprocal connection makes it difficult to restrict experimental manipulation to one specific side of the synapse or the other. Light can uniquely elicit feed-forward synaptic signals from photoreceptors, but eliciting a feedback signal specifically from the HCs has required intracellular manipulation of membrane potential with sharp electrodes or larger patch clamp pipettes. Practically speaking, these recordings can only be implemented in one or two cells at a time.

Optogenetics and chemogenetics have emerged as popular methods for perturbing membrane potential in entire populations of genetically-targeted cells without requiring insertion of electrodes (Atasoy and Sternson, 2018). While the intrinsic light-sensitivity of photoreceptors complicates the use of optogenetics in the retina, chemogenetics is well-suited for manipulating specific cell types without the use of light (Drinnenberg et al., 2018). Chemogenetics involves the exogenous expression of a receptor that is foreign to an organism's nervous system, with activation of the receptor brought about by an agonist that is also foreign and selective.

One such receptor is FaNaC, a rare example of a neuropeptide receptor that is not metabotropic, but an ionotropic (Na^+-selective) ion channel. FaNaC, which is normally expressed in mollusks but not in vertebrates (Golubovic et al., 2007), is activated by the neuropeptide Phe-Met-Arg-Phe-amide (FMRFamide), which is also absent from the vertebrate nervous system. In the mammalian brain, application of FMRFamide onto neurons genetically targeted to express FaNaC leads to depolarization and stimulation of action potential firing (Schanuel et al., 2008). PSAMs (pharmacologically selective actuator modules) are another type of foreign receptor. PSAMs were engineered specifically to operate orthogonally to natural chemical neurotransmission (Magnus et al., 2011). The PSAM used here was derived from a chimeric combination between the ligand-binding domain of a nicotinic acetylcholine receptor and the transmembrane domain of a Cl^--conducting glycine receptor (PSAM-GlyR), yielding an engineered ligand-gated Cl^- channel.

Transgenic zebrafish models are well-suited for exploring neural function, especially with respect to vision. Zebrafish have a short generation time, breed in large numbers, and are easy to maintain in laboratories. Molecular strategies developed over decades enable efficient generation of transgenic lines (Niklaus and Neuhauss, 2017). The transparency of zebrafish embryos enables functional *in vivo* imaging of the retina, brain, and spinal cord in completely intact animals (Dreosti et al., 2009). Zebrafish larvae can also be used for high throughput behavioral screens, taking advantage of their permeability to many small molecule drugs directly from the water in which they swim (Cassar et al., 2017).

Previous studies on zebrafish supported the hypothesis that a change in extracellular pH accounts for most of the *negative feedback* signal from HCs onto cones that underlies lateral inhibition (Wang et al., 2014; Kramer and Davenport, 2015). An as yet unidentified signal mediates *positive feedback* from HCs onto cones (Jackman et al., 2011), a process that amplifies lateral inhibition. Here, we utilize FMRFamide and PSAM-GlyR in transgenic zebrafish, targeted with cell-type specific promoters, to leap-frog over the photoreceptors and directly manipulate HC membrane potential. We examine the effects of HC manipulation at progressive downstream stages in retinal signaling, first at the level of synaptic exocytosis from cone photoreceptors, second at the level of postsynaptic responses of bipolar cells, and finally at the level of center vs. surround responses in RGCs.

MATERIALS AND METHODS

All animal procedures were performed in accordance with the Author University Animal Care and Use Committee regulations and were conducted in adherence to the Association for Research in Vision and Ophthalmology (ARVO) Statement for the Use of Animals in Ophthalmic and Vision Research as well as the Society for Neuroscience Policies on the Use of Animals and Humans in Neuroscience Research.

Animal husbandry

Adult or larval zebrafish (*Danio rerio)* of either sex were used in all experiments. Animals were housed in a recirculating water system at a density of 5-10 adult fish per 1 L water. Animals were reared at 27-28.5° C in mixed-sex groups of the same date of birth on a 14 h light, 10 h dark cycle. The Zeitgeber time of light onset at the animal facility was 09:00, and light offset was 23:00. Fish were bred no more than once per week. Water quality was checked twice daily for pH, temperature, and conductivity, and once weekly for nitrite, nitrate, alkalinity, and general hardness.

DNA constructs and transgenic fish

Transgenic zebrafish expressing FaNaC were generated as described elsewhere (Wang et al., 2014) (ZFIN Cat#ZDB-ALT-140924-3, RRID:ZFIN_ZDB-ALT-140924-3) and were activated using its cognate agonist FMRFamide (Sigma Aldrich, P4898; CAS Number 64190-70-1). PSAM expressing fish were generated specifically for this study (ZFIN Cat# ZDB-ALT-181031-3, RRID:ZFIN_ZDB-ALT-181031-3). The PSAML141F,Y115F:GlyR (RRID:Addgene_32480, Magnus et al., 2011) was sub-cloned into pDONR221 to obtain pME-PSAM-GlyR. For bicistronic expression of PSAM-GlyR with the green fluorescent protein eGFP, the coding sequence of the Internal Ribosome Entry Site (IRES) viral peptide was inserted at the 5' end of the eGFP coding sequence in p3E-eGFP to produce p3E-IRES:eGFP. To generate the PSAM constructs, we recombined p5E-MCS Cx55.5 (Shields et al., 2007) (kindly provided by Maarten Kamermans, Netherlands Institute for Neuroscience), pME-PSAM AA0416 Y115F-L141F-GlyR, p3E- IRES:eGFP and pDestTol2CG2 from the Tol2kit#395 (RRID:Addgene_63156) for making transgenic fish. One- or two-cell-stage zebrafish (*Danio rerio,* AB strain) embryos were microinjected with the DNA constructs together with Tol2 mRNA for a higher germline transmission rate (Kwan et al., 2007). The transgene-positive F0 founders were selected by screening for green heart fluorescence (myl7:GFP, aka cmlc2) in embryos at 2–4 days post fertilization (Kwan et al., 2007) and raised at 28.5 °C in a 14 h light, 10 h dark cycle. Adult F0 fish were inbred, and their transgene-positive progeny were screened by green heart fluorescence, raised, and used for imaging experiments and immunohistochemistry. The PSAM-GlyR is activated by its cognate agonist PSEM^{89S} (Tocris Biosciences; IUPAC name: N-(3S)-1-Azabicyclo[2.2.2]oct-3-yl-2,5-dimethoxybenzamide trifluoroacetate , CAS number: 1336913-03-1).

Transgenic zebrafish expressing GCaMP6f under the pan-neuronal promoter HuC [Tg2(elavl3:GCaMP6f), RRID:ZFIN_ZDB-GENO-180220-2, ZFIN Cat# ZDB-FISH-180220-12] were kindly provided by the Florian Engert Lab. To generate HuC:GCaMP and FaNaC double transgenic fish or HuC:GCaMP and PSAM-GlyR double transgenic fish, the HuC:GCaMP transgenic fish line was crossed with either the FaNaC or PSAM-glyR fish line. Double transgenic expression was confirmed by screening embryos at 3 days postfertilization (dpf) for concurrent

expression of a green fluorescent heart, and a green fluorescent nervous system (i.e. brain and spinal cord).

Tissue preparation

Fish were dark adapted for at least 30 minutes prior to dissection. Adults were killed by immersion in an overdose concentration of 400mg/L MS-222, with decapitation as a secondary means of euthanasia. Zebrafish larvae <7 dpf used for ERG recordings were killed by decapitation followed by pithing, and recordings were performed on isolated eyes. For experiments performed on isolated retinas**,** dark-adapted retinas were dissected and isolated from the enucleated eyes in the dark, under infrared light, using IR viewers connected to the dissection microscope. The retinal pigment epithelium was manually separated from the neurosensory retina. Retinas were maintained in darkness in bubbled bicarbonate-buffered saline. For flat-mount preparations, retinas were mounted onto a Biopore membrane (MILLIPORE) with photoreceptors facing the membrane (Koizumi et al., 2007).

For gramicidin-perforated recordings from isolated HCs, adult zebrafish retinas were dissected and prepared for HC dissociation as previously described (Nelson et al., 2008). Briefly, retinas were incubated for 1 hour at room temperature with gentle agitation in 1 ml of 0 Ca^{2+} saline (120 mM NaCl, 10 mM glucose, 2.5 mM KCl, 1.2 mM $MgSO_4$, buffered to pH 7.7 with 3 mM HEPES), containing 30 units of papain (Worthington Biochemical) activated with 1 mM cysteine, and 2 mg/ml hyaluronidase (Worthington Biochemical). Retinas were washed with Ca^{2+} (2.2 mM) saline solution containing 1% BSA to inactivate papain, and then gently triturated 3 times in saline solution and plated onto plastic coated 35 mm dishes, which served as the recording chamber.

Patch clamp recording

To measure responses to FMRFamide, $PSEM^{89S}$, GABA and muscimol, HC cells were recorded with the perforated patch configuration using gramicidin as the perforating agent. The bathing solution contained (in mM) 120 NaCl, 2.5 KCl, 1.2 $MgSO_4$, 2.2 $CaCl_2$, 3.0 HEPES, pH 7.7. A stock solution of gramicidin in ethanol (5 mg/ml) was prepared and diluted into the pipet solution (130 mM KCl, 3 mM NaCl, 10 mM HEPES, pH 7.4) at a ratio of 6 µl/ml. Pipets were pulled to a resistance of approximately 10-12 MOhms using a vertical puller (PC-100, Narishige Scientific Instruments). Following seal formation, the presence of a membrane potential in the current clamp recording configuration confirmed successful perforation, usually within the first minute. $PSEM^{89S}$ (500 µM), GABA (1 mM) and muscimol (100 µM) were applied with 100 ms pulses of positive pressure (1-2 psi) from a second pipet positioned approximately 100 µm from the cell. FMRFamide (30 µM) was bath applied for 5 minutes prior to measuring changes in membrane potential. FMRFamide was purchased from Sigma-Aldrich. Other agonists were purchased from Tocris Biosciences. Recordings were made using the MultiClamp 700b patch clamp amplifier ,

and pClamp software (Molecular Devices). All reported values were corrected for junction potentials, calculated using pClamp software.

FM1-43 imaging experiments

We used the fluorescent amphipathic dye FM1-43 to quantify synaptic exocytosis from cone photoreceptor terminals, as described previously (Rea et al., 2004; Choi et al., 2005). First, the isolated retina was treated with FM1-43 (30 µM) in normal saline containing (in mM) 100 NaCl, 2.5 KCl, 1 $MgCl_2$, 1 $CaCl_2$, 0.4 ascorbic acid, 20 dextrose and 25 $NaHCO_3$ bubbled with 5% CO_2 and 95% O_2 at 21°C for 15 minutes in darkness. This allows dye to accumulate in recycling synaptic vesicles. The loading period was followed by a 15 min wash with 0 Ca^{2+}, 1 mM EGTA saline to suppress premature unloading of dye by Ca^{2+}-dependent exocytosis. Residual dye trapped in the surface membrane was removed with Advasep-7 (1 mM) (Kay et al., 1999). After the wash period , Ca^{2+}-free saline was replaced with normal Ca^{2+}-containing saline to allow Ca^{2+}-dependent exocytosis of dye-loaded vesicles, leading to loss of FM1-43 fluorescence. Dye loss was visualized with 2-photon microscopy, and the decrease in fluorescence intensity over time was normalized to the initial fluorescence, before adding back Ca^{2+}. At the end of each experiment, high K^+ saline (50 mM KCl, iso-osmotically replacing NaCl) was applied for 15 min to elicit exocytosis of all releasable vesicles. Any remaining background fluorescence, attributable to dye trapped in unreleasable compartments, was normalized to zero.

Two-photon imaging was carried out with a Zeiss 510 microscope equipped with a MaiTai (Spectra Physics, Mountain View, CA) mode-locked Ti:sapphire laser (860 nm) and a 40× achroplan, 0.8 NA water-immersion objective. Images were acquired at a frame rate of 10 Hz with Zeiss LSM software and analyzed with Scion Image software. Continuous imaging of FM1-43 resulted in some degree of steady state light adaptation (Choi et al., 2005). Optical sections focused 300 nm apart were obtained to image throughout the thickness of the outer plexiform layer (OPL). Z-stacks encompassing the entire OPL were corrected for drift and summed with FiJi ImageJ to generate average intensity z-projections.

Electroretinogram recordings (ERGs):

Corneal ERGs were recorded from dark-adapted eyes isolated from <8 dpf zebrafish larvae in oxygenated Ringer's solution. Animals were dark adapted for at least 12 hours prior to experiments. ERGs were recorded from isolated eyes on filter paper by using a glass pipette (G150TF-4, Warner Instruments) pulled to a diameter of 10-12 micrometers (Flaming/Brown type micropipette puller, Sutter Instruments, P-97) placed onto the central cornea with a hydraulic micromanipulator. Each pipette tip was individually examined and smoothed as needed (MF-83 microforge, Narishige Scientific Instruments). A platinum wire placed beneath the moist filter paper was used as a reference electrode. Monochromatic light was presented to eyes via a monochromator with a 150-W Xenon high stability lamp (Polychrome V, Till

Photonics GmbH, Graefelfing, Germany). Three repetitive 2-second isoluminant pulses of 400 nm light with 15 second interstimulus intervals were used to elicit ERG responses and were averaged for each of 8 measured time points. FMRFamide or PSEM^{89S} was added at t=0min. The b-wave amplitude was measured by subtracting the baseline value or the minimal value of the first negative peak to the maximal value of the first positive peak (Evers and Gouras, 1986). For comparisons between treatment groups, the ERG was normalized to the b-wave peak amplitude prior to drug application. Data were acquired and processed with a custom-written Matlab routine. Wild type (WT) AB-strain zebrafish or transgene-negative larvae of the same spawning were used for control experiments.

GCL calcium imaging

For 2-photon Ca^{2+}-imaging experiments, we used a transgenic zebrafish expressing the genetically encoded calcium indicator GCaMP6f, under the control of a pan-neuronal promoter (HuC). Whole retinas were isolated from dark-adapted adult zebrafish and flat-mounted on Biopore membrane with the RGC side facing the top of the chamber. Retinas were continuously perfused with bicarbonate-buffered solution containing (in mM) 100 NaCl, 2.5 KCl, 1 MgCl2, 1 CaCl2, 0.4 ascorbic acid, 20 dextrose and 25 NaHCO3 bubbled with 5% CO2 and 95% O2. We focused on a single image plane in the ganglion cell layer and used ImageJ (rsbweb.nih.gov/ij) to define regions of interest, corresponding to individual somata. We used 920 nm light for GCaMP6f 2-photon excitation. Emitted light was passed through a 530 nm barrier filter.

Immunohistochemistry

Transgenic and WT zebrafish of either sex were dark adapted, killed as previously detailed and their eyes were enucleated. For tissue fixation 4% paraformaldehyde was prepared from 100% paraformaldehyde diluted in 1xPBS buffered to a pH of 7.4. The eyes were fixed for at least 1 hour. After fixation the eyes were rinsed in PBS, and cryoprotected by immersion for 1 hour in 15% sucrose followed by one hour in 30% sucrose solutions. Eyes were sectioned at a thickness of 14 microns using a microtome (Thermo Fisher Microm HM550) and kept in a -20° C freezer until immunohistochemistry was performed.

Immunohistochemistry using an antibody to GFP was performed to enhance detection of labeling in PSAM-GlyR fish. Details have been reported elsewhere (Beckwith-Cohen et al., 2019). Briefly, sections were incubated for 30 minutes at 4° C in blocking solution consisting of 1% Triton x-100 (Sigma Aldrich), 1% bovine serum albumin fraction V (MP Biomedicals LLC, 160069) at 4° C . Sections were rinsed in PBS, and then incubated with mouse anti-GFP monoclonal unconjugated antibody (ABCAM ab1218) at a 1:400 dilution and blocking solution for two hours. After washing, sections were immersed in 4° C blocking solution including AlexaFluor 488 goat anti-mouse igG (ThermoFisher Scientific, catalog #A-11001) at a 1:1000

dilution with gentle agitation for 1 hour at 100 rpm. Sections were then rinsed again for 3 cycles in chilled PBS, air dried and sealed using Fluoromount-G with DAPI mounting solution (Invitrogen). Negative controls included sections of the same tissue without the primary antibody. Sections were imaged using a confocal microscope (Carl Zeiss LSM880). GFP and mCherry were excited at 488 nm and 647 nm using Argon and HeNe lasers respectively; DAPI was excited using ultraviolet light at 348 nm. Live larval images were obtained from 1-3 dpf zebrafish larva embedded in agarose gel as previously described (Williams et al., 2013). Larvae were imaged using a confocal microscope (Carl Zeiss LSM880).

Statistical analysis

Statistical significance for sample numbers less than ten was determined by using the two-sided nonparametric Mann-Whitney *U* test. Significance for multiple group comparisons was determined using one-way ANOVA followed by the two-tailed Student's *t* test. Significance was otherwise determined by two-tailed Student's *t* test. Effects were considered significant at p values less than 0.05. Data points and error bars represent the mean ± s.e.m. Statistics were performed using Microsoft Office Professional Excel version 2016, or Matlab 9.

RESULTS

Chemogenetic tools for manipulating horizontal cells

To use a chemogenetic approach to manipulate HC membrane potential, we used two zebrafish lines. One was a previously developed transgenic line (Wang et al., 2014) that expresses the FMRFamide-activated Na^+ channel (FaNaC) from the snail *Helix aspersa*. FaNaC expression was controlled by the connexin 55.5 promoter, which in the retina, enables specific expression in HCs (Shields et al., 2007). The transgenic insert also encoded the fluorescent protein mCherry, which allowed us to verify that the only retinal cells expressing FaNaC were HCs (Fig. 1A). We developed a second transgenic zebrafish line that expresses the Pharmacologically Selective Actuator Module on the Glycine Receptor (PSAM-GlyR) (Magnus et al., 2011). PSAM-GlyR was also expressed under the control of the connexin 55.5 promoter, along with eGFP to allow visualization of cells expressing the alien channel (Fig. 1B). Because PSAM-GlyR is a Cl^- channel, the effect of $PSEM^{89S}$ on membrane potential is dependent on the value of E_{Cl}, which varies depending on the concentrations of Cl^- in the bathing solution and in the patch pipette. Binding of the designer agonist $PSEM^{89S}$ to PSAM-GlyR should open Cl^- channels and drive the membrane potential towards E_{Cl}.

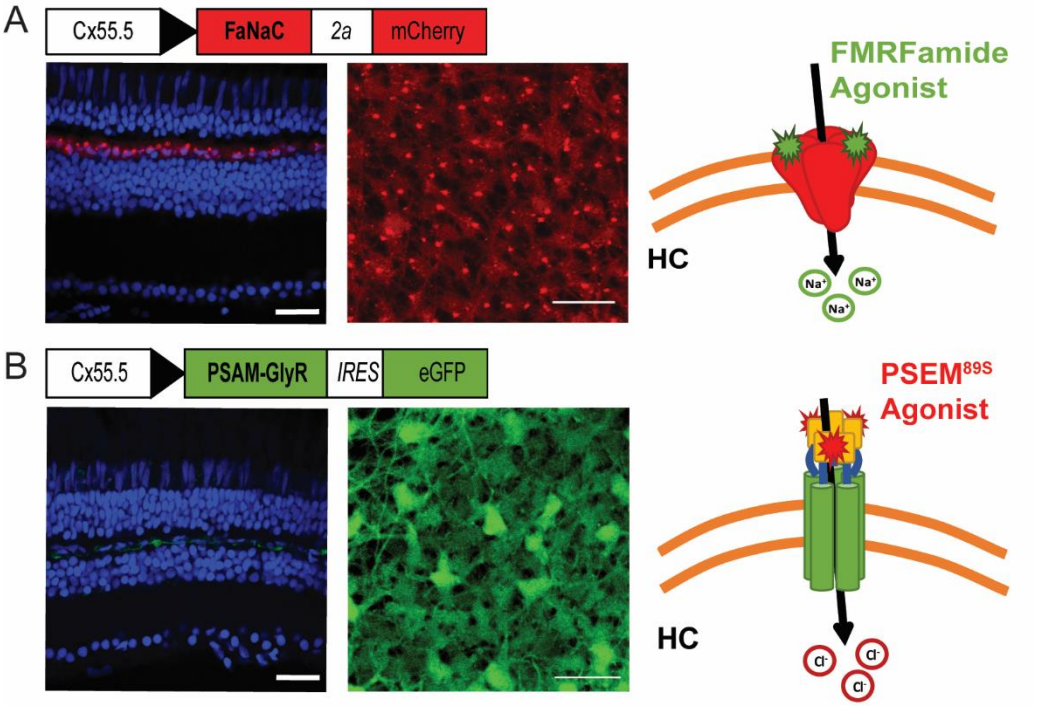

Figure 1: Strategy for chemogenetic manipulation of horizontal cell membrane potential.

(A) A bicistronic construct containing the molluscan FMRFamide-activated Na^+ channel (FaNaC) from *Helix aspersa* and the red fluorescent protein mCherry, both under the control of the Cx55.5 promoter, were transgenically expressed in HCs of zebrafish causing red fluorescence specific to the HC layer. mCherry exhibits intrinsic fluorescence seen in confocal imaging of a fixed retinal section (left) and in 2-photon imaging of a fresh retinal flat mount (right). Puncta with saturating expression of mCherry likely represent protein aggregates within the Golgi apparatus of HCs. A diagram illustrates how binding of the agonist FMRFamide causes Na^+ influx thereby depolarizing the membrane potential. (B) A bicistronic construct containing the Pharmacologically Selective Actuator Module on the Glycine Receptor (PSAM-GlyR) and the green fluorescent protein eGFP, both under the control of the Cx55.5 promoter, were transgenically expressed in HCs of zebrafish causing green fluorescence specific to the HC layer. eGFP was immunolabeled with AlexaFluor 488 for confocal imaging of a fixed retinal section (left) and its intrinsic fluorescence is seen in 2-photon imaging of a fresh retinal flat mount (right). A diagram illustrates how binding of the designer agonist $PSEM^{89S}$ causes Cl^- influx thereby clamping the membrane potential to E_{Cl}. Nuclei are stained with DAPI (blue). Scale bar is 20 µm.

To determine how activation of the PSAM-GlyR receptor changes HC membrane potential, we used the perforated patch recording technique in which an ionophore added to the pipette solution inserts into the plasma membrane, providing access for measuring intracellular voltage. Gramicidin was chosen as the perforating agent as it forms cation channels that are impermeant to Cl^-, thus preserving the normal internal Cl^- concentration (Kyrozis and Reichling, 1995). As our access resistance was typically about 100 MOhms, we measured HC responses to agonists without attempting to manipulate membrane voltage with extrinsic current. A typical response to a 100 ms puff of $PSEM^{89S}$ is shown in Figure 2A. $PSEM^{89S}$ consistently hyperpolarized HCs, ranging from -3.0 to -9.1 mV (n=6). Overall, $PSEM^{89S}$ reversibly hyperpolarized HCs from a mean resting potential of -43.7 ± 1.6 mV to an average potential of -49.28 ± 1.0 mV (Figure 2D). This finding is consistent with an E_{Cl} value more negative than the

resting potential, resulting in hyperpolarization upon activation of PSAM-GlyR. Application of PSEM^{89S} had no effect on cells from wildtype zebrafish (n=10, data not shown).

Previous studies showed that the inhibitory neurotransmitter GABA can lead to depolarization of HCs (Miller and Dacheux, 1983; Djamgoz and Laming, 1987; Kamermans and Werblin, 1992; Grove et al., 2019). To better understand this process, we puffed GABA onto HCs and recorded membrane potential responses. Some HCs hyperpolarized (2.6 ± 0.4 mV, n=5), some depolarized (3.6 ± 0.8 mV, n=4), and some exhibited a biphasic response (n=2) (Figure 2B). The complex response suggests multiple conductance mechanisms activated by GABA. Fish HCs possess highly Cl^--selective $GABA_A$ receptors (Gilbertson et al., 1991; Kamermans and Werblin, 1992; Takahashi et al., 1995; Paik et al., 2003), but they also express GABA transporters (Malchow and Ripps, 1990; Cammack and Schwartz, 1993; Dong et al., 1994; Kreitzer et al., 2003; Nelson et al., 2008) which have a GABA-activated Na^+-conducting pore (Krause and Schwarz, 2005). To test whether $GABA_A$ receptor activation is hyperpolarizing in HCs, we used muscimol, which is highly specific for $GABA_A$ receptors and has no effect on GABA transporters (Malchow and Ripps, 1990). We found that muscimol produced only hyperpolarizing responses (Figure 2C, n=7, range of -1.2 to -3.3 mV). Responses to GABA and muscimol are summarized in Figure 2E. Hence, the natural neurotransmitter GABA activates both a depolarizing transporter current and a hyperpolarizing $GABA_A$ current, with the net effect determined by the relative abundance or distribution of these targets. In contrast, the PSEM^{89S}/PSAM-GlyR system exclusively hyperpolarizes HCs, making it a particular effective tool for imparting inhibition.

Finally, we measured the effect of FMRFamide (30 µM) on HC membrane potential. HCs depolarized from -48.5mV ± 8.1mV (n=7 cells) at rest to -11.6 mV ± 7.8 mV upon application of FMRFamide, consistent with an increase in Na^+ conductance (Figure 2F). Thus, FMRFamide mediated activation of FaNaC is an effective tool for depolarizing HCs.

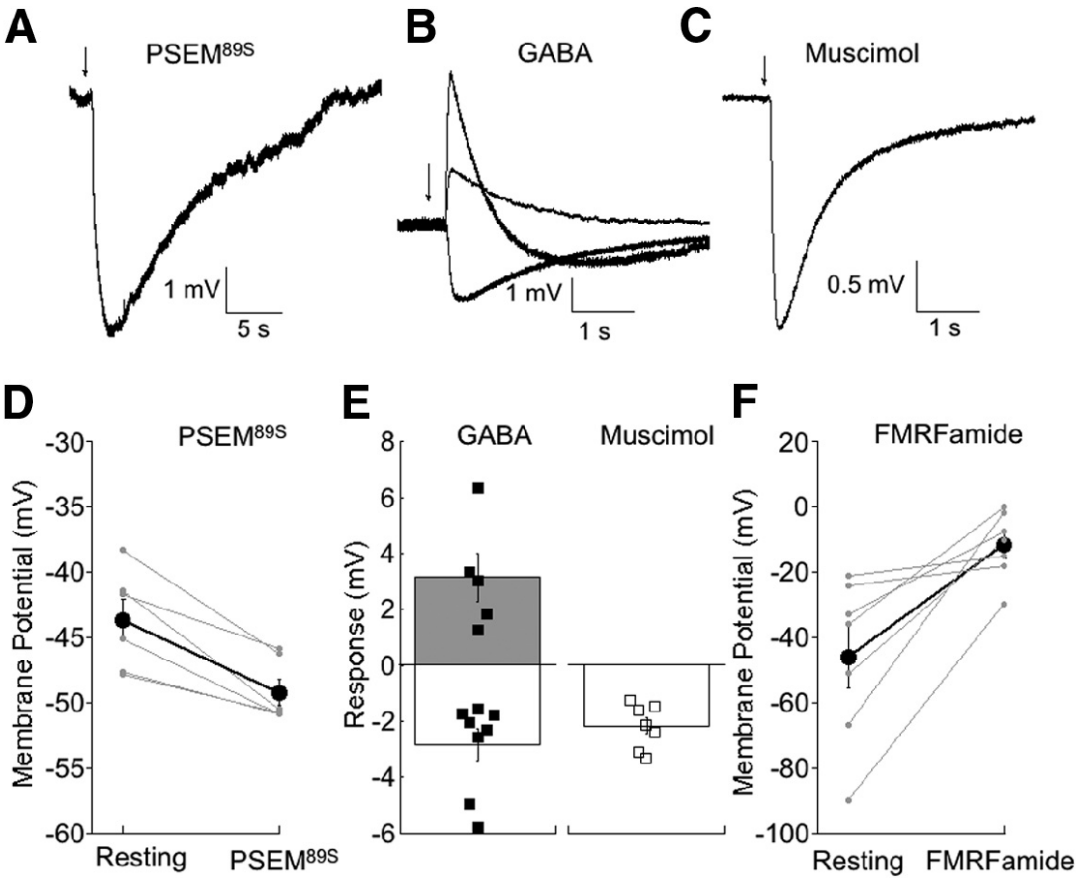

Figure 2: Monitoring changes in membrane potential elicited by FMRFamide and PSEM^{89S}.

(A) Voltage response to a 100 ms puff of PSEM^{89S} (500 µM) in an isolated HC recorded with the gramicidin perforated patch configuration. A Puff was delivered at the time indicated by the arrow. Although the concentration of PSEM^{89S} was 500 µM in the pipette, the concentration of the drug is estimated to be diluted ~50 fold at the cell (Firestein and Werblin, 1989), positioned approximately 100 µm from the puffer pipette. (B) Traces from 3 different HCs showing responses to 100 ms puffs of GABA (1 mM), chosen to highlight the variability of responses to GABA that were observed between cells. (C) Response to 100 ms application of muscimol (100 µM), a $GABA_A$ receptor agonist. Responses were uniformly hyperpolarizing in all cells tested. (D) Summary data showing the resting membrane potential, and the membrane potential at the peak of the response to PSEM^{89S}. Large bolded symbols are the mean±sem for each condition (n=6). (E) Summary of the change in membrane potential evoked by puffs of GABA or muscimol. Small closed symbols are the responses of individual cells to GABA (n=11). Open symbols are the responses to muscimol (n=7). Open boxes are the mean±sem for hyperpolarizing responses, and the shaded box is the mean±sem for depolarizing responses. The mean amplitude of the responses evoked by muscimol was not significantly different from the amplitude of hyperpolarization evoked by GABA (p=0.53, Rank Sum Test). (F) Summary data for bath application of FMRFamide (30 µM). Large bolded symbols are the mean±sem for each condition (n=7).

Chemogenetic manipulation of HCs alters FM1-43 destaining of cone terminals.

To measure tonic exocytosis from photoreceptors, we used the synaptic vesicle dye FM1-43 (Betz and Bewick, 1992). FM1-43 is an amphipathic molecule that becomes fluorescent when it inserts itself into the plasma membrane. The dye is then washed off the tissue, with residual fluorescence attributable to dye trapped within vesicles internalized by endocytosis (Rea et al.,

2004). Synaptic exocytosis releases the dye, causing a gradual decrease in tissue fluorescence. Photoreceptor terminals exhibit tonic exocytosis in darkness, resulting in progressive spontaneous release of dye.

Previous work (Jackman et al., 2011) suggests that two distinct events initiate negative or positive feedback from HCs to cone photoreceptor terminals, as illustrated in Figure 3A. Negative feedback is initiated by a change in HC membrane potential, leading to a change in extracellular proton concentration. This modulates the gating of voltage-gated Ca^{2+} channels in cone terminals, thereby regulating Ca^{2+}-dependent exocytosis. Positive feedback is initiated by a local change in intracellular Ca^{2+} in the dendrites of HCs, a process that depends on a change in influx through Ca^{2+}-permeable AMPA receptors. The positive feedback signal is still unidentified, although it is known that it too regulates Ca^{2+}-dependent exocytosis from photoreceptors. According to this model, altering membrane potential of HCs by activating chemogenetic tools should affect negative feedback, but not positive feedback, which is dependent on Ca^{2+} influx through AMPA receptors.

To test this prediction, we measured the cone terminal FM1-43 unloading rate in darkness, in retinas from both FaNaC and PSAM-GlyR fish. In fully dark-adapted FaNaC fish retina with no agonist added, destaining occurred at 0.87 ± 0.08 % per minute (Figure 3C, D, n=10 retinas). The FM 1-43 destaining rate increased with AMPA (1.89 ± 0.13 %, n=9 retinas, $p < 1 \times 10^{-5}$ compared with no agonist) and slowed with FMRFamide (0.54 ± 0.07 % n=9 retinas, $p = 0.001$ compared with no agonist) while adding FMRFamide and AMPA together resulted in a destaining rate that was not different than with AMPA alone (1.96 ± 0.25 %, n=4, $p = 0.88$).

In PSAM-GlyR fish, the destaining rate with no agonists added was 0.41±0.12 % per minute (Figure 3E). The slower measured destaining rate as compared to FaNaC retina was attributed to a shorter period of dark adaptation before beginning the imaging session. In the presence of the agonist $PSEM^{89S}$ (30 µM), the destaining rate increased to 0.83±0.19 %, significantly faster than the rate in the absence of agonist (Figure 3F, n=9 retinas, $p = 0.044$). Addition of 20 µM AMPA significantly increase the FM 1-43 unloading rate compared to dark control (2.19 ± 0.19 %, n=5 retinas, $p = 0.0002$). The addition of both 30 µM $PSEM^{89S}$ and 20 µM AMPA resulted in an acceleration similar to that seen with AMPA alone (2.05 ± 0.35 %, n=5, $p = 0.82$) (Figure 3F).

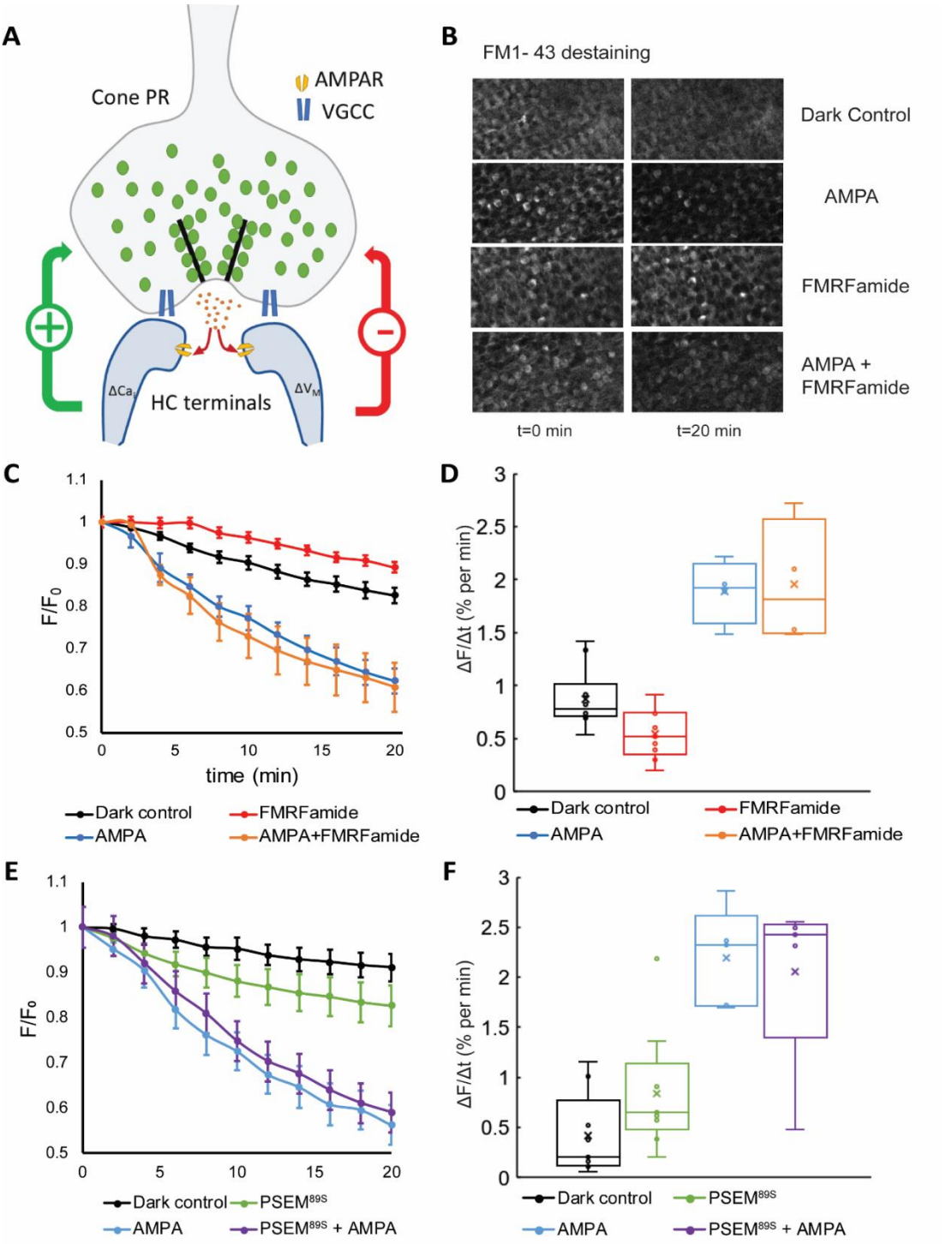

Figure 3: Chemogenetic activation of HCs alters vesicular release of FM1-43 from cone terminals.

(A) Schematic representation of the mechanisms of negative (-) and positive (+) feedback of HCs onto cones. VGCCs are voltage-gated Ca^{2+} channels, green circles are FM1-43-filled synaptic vesicles, orange dots are glutamate molecules in the synaptic cleft, AMPARs are AMPA receptors. Negative feedback is mediated by changes in the membrane potential of HCs, whereas positive feedback is mediated by increased intracellular Ca^{2+} in HCs, owing to influx of Ca^{2+} through Ca^{2+}-permeant AMPA receptors. (B) 2-photon scanned images of the photoreceptor

terminal layer in FaNaC zebrafish retinas. Retinas were pretreated with FM1-43 to load recycling synaptic vesicles and then treated for 20 min with the indicated receptor agonist. AMPA (20 μM) increased the rate of dye loss (destaining) and FMRFamide (10 μM) decreased destaining, but the AMPA-elicited increase was dominant when the two agonists were applied together. (C, D) Time course of FM1-43 destaining in FaNaC fish. Without added agonists, cone terminals released FM1-43 at 0.87 ± 0.08 % per minute (n=10 retinas). Adding AMPA accelerated destaining rate (1.89 ± 0.13 %, n=9 retinas, $p < 1 \times 10^{-5}$). Adding FMRFamide (10 μM) decelerated destaining (0.54 ± 0.07 % n=9 retinas, $p = 0.001$). Adding AMPA and FMRFamide together resulted in a significant destaining rate from dark ($p = 0.002$), which was not significantly different than that with AMPA alone (1.96 ± 0.25 %, n=4, $p = 0.88$). Statistical differences were determined with one-way ANOVA ($F_{(3,23)} = 27.4$, $p = 8.9 \times 10^{-8}$). (E, F) Time course of FM1-43 destaining in PSAM fish. Adding PSEM^{89S} (30 μM) accelerated destaining by (0.83±0.19 %, n=9 retinas, $p = 0.044$). Adding AMPA accelerated destaining (2.19 ± 0.19 %, n=5 retinas, $p = 0.0002$). Adding PSEM^{89S} and AMPA together resulted in a destaining rate not significantly different than that with AMPA alone (2.05 ± 0.35 %, n=5, $p = 0.82$). Analysis was performed with one-way ANOVA ($F_{(3,24)} = 14.69$, $p = 1.2 \times 10^{-5}$).

Chemogenetic manipulation of HCs reduces the b-wave of the ERG.

Chemogenetic manipulation of HC feedback onto cones should have consequences on the responses of downstream neurons in the visual system, starting with alteration of postsynaptic responses in the outer retina. The ERG b-wave reflects light-elicited synaptic currents, originating primarily in bipolar cells (Stockton and Slaughter, 1989). Following establishment of a stable baseline in control solution, either FMRFamide (10 μM) or PSEM^{89S} (30 μM) was added to the bathing solution. Isolated eyes from WT fish had ERGs that were unaffected by FMRFamide (0.97±0.11, n=10, $p = 0.92$) (Figure 4A). However, in FaNaC fish, FMRFamide decreased the ERG b-wave (Figure 4B, C) (0.63±0.06, n=9, $p = 0.007$). The effect of FMRFamide on the b-wave was prevented by adding 20 mM HEPES (1.08±0.11, n=7, $p = 0.92$), thus supporting the pH mediated effect that horizontal cells have on retinal light responses (Wang et al., 2014; Beckwith-Cohen et al., 2019). The FMRFamide effect was dose-dependent with an EC_{50} of 4.25μM (Figure 4D), consistent with previous estimates of the affinity of FaNaC for the neuropeptide (Schanuel et al., 2008).

ERGs from WT fish were also unaffected by PSEM^{89S} (30 μM) (n=8, 0.96±0.03, $p = 0.703$) (Figure 4F). However, in PSAM-GlyR fish, PSEM^{89S} decreased the b-wave (Figures 4E-F, n=7, 0.84±0.05, $p = 0.025$). This effect was smaller than that of FMRFamide on FaNaC fish, but nonetheless statistically significant. Without agonist, the ERG of PSAM-GlyR fish was indistinguishable from that of WT fish.

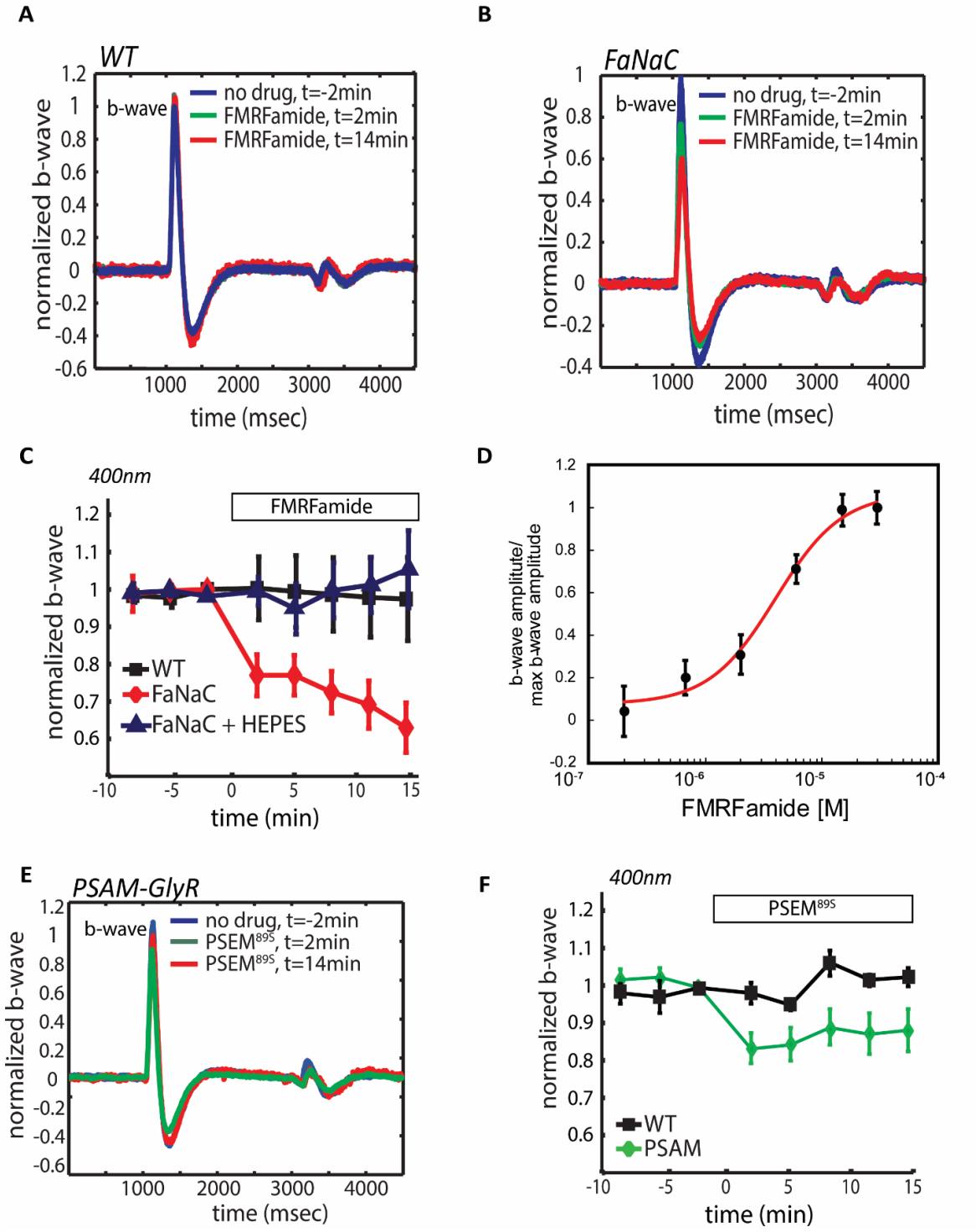

Figure 4: Chemogenetic manipulation of HCs modulates the bipolar cell light response.

Application of FMRFamide had no effect on the ERG of WT zebrafish (A), but decreased the maximal b-wave amplitude in FaNaC zebrafish (B), reaching a maximum ~40% decrease in the b-wave (C). Application of the buffer HEPES (pH=7.35) cancelled the effects of FMRFamide (C). FMRFamide response was dose dependent having an EC_{50} of 4.25µM (D). Application of the agonist $PSEM^{89S}$ (30 µM) also caused a decrease in the maximal b-wave amplitude, but to a lesser degree (E-F).

Chemogenetic manipulation of HCs disrupts surround inhibition in RGCs.

RGCs display an antagonistic center vs. surround receptive field, mediated in large part by lateral inhibition in the outer retina. Chemogenetically manipulating the membrane potential of HCs should alter lateral inhibition and therefore change the degree of surround antagonism in RGCs, similar to the effect of pH buffers that disrupt HC signaling (Davenport et al., 2008). To measure RGC responses, we used a transgenic zebrafish expressing the genetically encoded calcium indicator GCaMP6f, under the control of a pan-neuronal promoter (HuC). We observed GCaMP6f expression throughout the nervous system *including* the brain, spinal cord, and retina (Figure 5A-D). Two-photon Ca^{2+} imaging was used to measure RGC responses to light stimuli (Fig 5B).

GCaMP6f fish were crossed with FaNaC or PSAM-GlyR fish to create double transgenic fish lines. In embryos treated with PTU to prevent pigmentation, GCaMP6f could be seen in developing RGCs *in vivo* at 1 dpf. mCherry, a co-expression marker for FaNaC, could be seen *in vivo* in HCs at 2 dpf (Fig. 5D). eGFP, a co-expression marker for PSAM-GlyR, could not be detected concurrently with GCaMP6f because of spectral overlap, although expression was confirmed in intact retinas by immunohistochemistry (Fig. 1B) and in dissociated HCs.

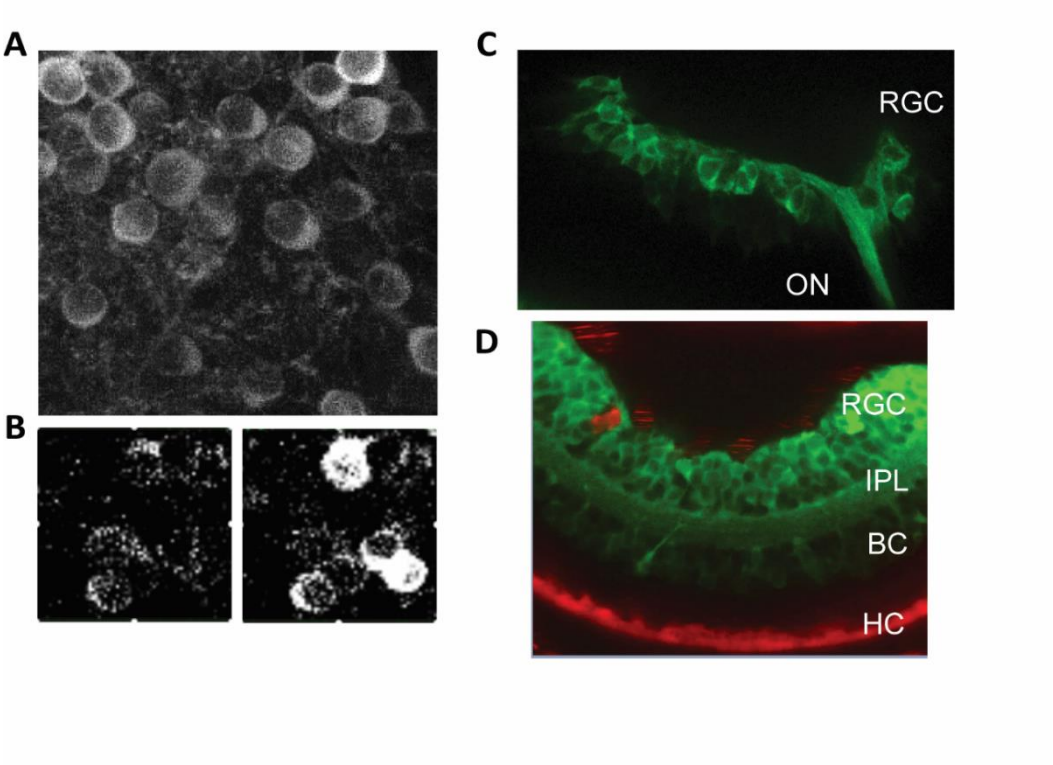

Figure 5 Expression of GCaMP6f in chemogenetic zebrafish lines.

(A) *Ex vivo* retina of adult HuC-GCaMP6f zebrafish shows eGFP fluorescence in retinal flat mounts using 2-photon imaging. (B) Light response is easily measured in RGCs before (left) and after (right) a light flash. (C) *In vivo* confocal imaging of eGFP in 1 dpf PTU-treated zebrafish larvae of HuC-GCaMP6f and FaNaC crossed transgenic fish. The optic nerve (ON) and the developing retina (RGC) show strong eGFP fluorescence. (D) *In vivo* imaging of the same

line of fish imaged in (C) showing that FaNaC-mCherry is easily visualized in HCs at 2 dpf zebrafish larvae. Some red autofluorescence is generated by scattered pigment cells on the ocular surface. RGC- retinal ganglion cell layer, IPL- inner plexiform layer, BC- ipolar cell layer, HC- horizontal cell layer.

To measure RGC responses, three repeated light stimuli were delivered at each of six spot diameters (ranging 50-1000µm) and Ca^{2+} transients were recorded using 2-photon imaging (Figure 6A). In WT-GCaMP6f the Ca^{2+} response grew with increasing spot diameter (n= 16), but only up to a point. The Ca^{2+} signal reached a maximum at 500µm (Figure 6B), and then decreased with a larger spot (1000µm), consistent with surround antagonism (Vessey et al., 2005; Davenport et al., 2008; Klaassen et al., 2011). We calculated the lateral inhibition ratio (LIR), defined as the response at 500µm/response at 1000µm. The LIR was 1.41±0.21 for WT. Addition of 20mM HEPES reduced this effect, resulting in an LIR of 0.95±0.09, (n= 8, p = 0.08). Applying 10µM FMRFamide had no effect on the LIR of WT fish (1.32±0.19, n= 14, p = 0.76) (Figure 6B). FaNaC retinas had surround inhibition prior to agonist application with an LIR of 1.76±0.26. Application of FMRFamide on FaNaC retinas reduced surround inhibition, resulting in an LIR of 0.78±0.04 (n= 4, p = 0.002) (Figure 6C). Likewise, PSAM-GlyR retinas displayed strong surround inhibition prior to agonist application (LIR = 1.49±0.09), and this surround inhibition was significantly reduced by application of $PSEM^{89S}$ (LIR = 1.04±0.08, n= 8, p = 0.0006; Figure 6D), suggesting that activation of PSAM-GlyR channels that are selectively expressed in horizontal cells also perturbed normal center surround responses of downstream RGCs. A summary of the LIR values in various conditions is shown in Figure 6E.

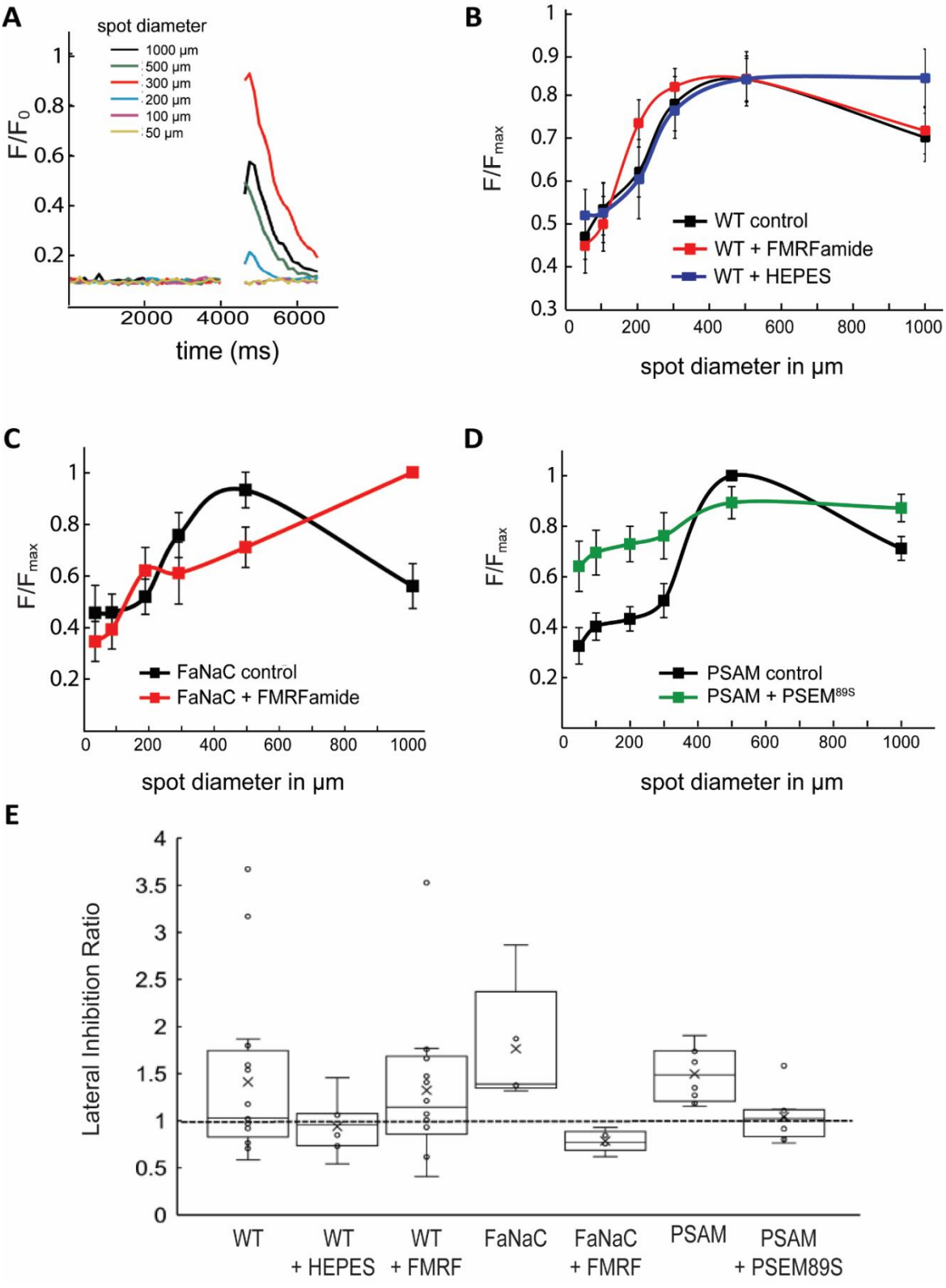

Figure 6: Chemogenetic manipulation of HCs alters lateral inhibition in downstream RGCs.

(A) Light responses were measured in HuC::GCaMP6f fish with three light stimuli, delivered at six different spot diameters. Calcium transients were recorded using fluorescence imaging. (B) WT RGCs responded with maximum change in fluorescence to a 500 µm spot of light, which decreased at 1000 µm, supporting lateral inhibition. This effect was blocked by HEPES, and was unchanged by applying 10 µM FMRFamide. (C) Application of FMRFamide on FaNaC retinas perturbed normal RGC center surround response, (D) as did application of $PSEM^{89S}$ on PSAM-GlyR retinas. (E) The lateral inhibition ratio (LIR) in various conditions shows that application of the cognate agonists to FaNaC and PSAM retina significantly disrupts lateral inhibition.

DISCUSSION

In the dark, photoreceptors are depolarized, eliciting a maximal release of glutamate, which acts through a sign conserving synapse on horizontal cells. A light stimulus slows synaptic release thereby hyperpolarizing HCs. Hyperpolarization of HCs in turn activates a negative feedback mechanism that helps restore the rate of transmitter release in the face of continuous light stimulation. Understanding both the mechanisms and the functions of HC feedback to photoreceptors is complicated by the reciprocal nature of the synapse. Chemogenetic tools enable direct manipulation of HC membrane potential, bypassing the photoreceptors to enable functional analysis of feedback. We first examined the effect of HCs on cone vesicular release. Because the Na^+ equilibrium potential (near +50 mV) is more positive than the HC resting potential (near -40 mV), application of FMRFamide should trigger Na^+ influx and depolarize cells expressing FaNaC, as we observed in dissociated HCs. This, in turn, should lead to decelerated vesicular release from cones, a prediction that is consistent with our finding that FMRFamide slowed FM1-43 destaining. Our result implies that depolarization of HC alone, through the use of chemogenetics, is sufficient to decrease transmitter release rates from cones. A role for the membrane potential of HCs in the modulation of photoreceptor transmitter release has been demonstrated elsewhere, although the precise underlying mechanism remains elusive (Vessey et al., 2005; Klaassen et al., 2011).

The small increase in FM1-43 release rate that we observed upon application of $PSEM^{89S}$ to PSAM-GlyR retina is consistent with a modest hyperpolarization of the HC membrane potential. As PSAM-GlyR is a Cl^- channel, hyperpolarization is expected if E_{Cl^-} is more negative than the HC resting potential. In agreement with this prediction, we observed consistent hyperpolarizing responses to $PSEM^{89S}$ in dissociated HCs when the normal intracellular Cl^- environment was preserved with gramicidin perforated patch recording. We also observed consistently hyperpolarizing responses when we used the specific agonist muscimol to activate $GABA_A$ receptors, which are highly Cl^--selective.

In contrast, application of GABA had complicated effects, in some cases, depolarizing HCs, and in others, generating a biphasic response. This is consistent with GABA activating more than one target. HCs express GABA transporters, which, in addition to shuttling the neurotransmitter, have a ligand-gated Na^+-selective pore, and would thus cause membrane depolarization (Malchow and Ripps, 1990; Cammack and Schwartz, 1993; Dong et al., 1994;

Kreitzer et al., 2003; Krause and Schwarz, 2005; Nelson et al., 2008). In fish horizontal cells, Blockade of the Cl^- pore of $GABA_A$ receptors with picrotoxin has a relatively small effect on the GABA response of HCs, suggesting that most of the current is mediated by the transporter (Malchow and Ripps, 1990; Cammack and Schwartz, 1993; Kreitzer et al., 2003; Nelson et al., 2008). Thus, the response to GABA is due to the simultaneous activation of a Na^+ transport current and a Cl^- current, mediated by the $GABA_A$ receptor.

To test whether manipulating HC membrane potential altered postsynaptic responses in downstream neurons in the outer retina, we measured responses to light flashes with ERGs. For these experiments we made use of the larval zebrafish (<8 dpf) which has several advantages compared with adult fish. First, a surface electrode on the cornea is sufficient to detect responses in the larvae, while measurements in the adult require perforation of the eye. Moreover, pharmacological agents can easily penetrate larval zebrafish. Thus, FMRFamide and $PSEM^{89S}$ can be applied to the retina and light responses can be recorded without interfering with ocular integrity. Although the ERG of zebrafish larvae does not fully mature until 21-24 dpf, a strong b-wave response to ultraviolet light occurs at 4-5 dpf (Saszik et al., 1999). The minimal a-wave seen in our ERGs (Fig 3A, B, E) is typical of the cone-dominant retina of larval zebrafish, which have yet to develop rods (Seeliger et al., 2002).

Application of either FMRFamide or $PSEM^{89S}$ in the appropriate transgenic zebrafish line, decreased the ERG b-wave, which is thought to reflect synaptic responses primarily from ON-bipolar cells. In principle, there are several ways that HCs might contribute to the b-wave of the ERG. First, synaptic currents in the HCs themselves might add to the trans-retinal electrical field in a way that could be detected in the ERG recording, contributing in a direct manner. This seems unlikely, as selective block of ON-bipolar cell light responses with L-AP4 eliminates the b-wave (Stockton and Slaughter, 1989; Thoreson and Miller, 1994; Robson and Frishman, 1995; Saszik et al., 2002). Second, feed-forward synapses from HCs to bipolar cells might also generate a synaptic current that directly contributes to the b-wave. While such a feed-forward connection has long been sought, evidence for a substantial synaptic response in bipolar cells that can be attributed to HCs remains scant, but cannot be ruled out (Thoreson and Mangel, 2012). Finally, feedback from HCs onto rod and cone photoreceptors will modulate their neurotransmitter release and alter responses of bipolar cells in an indirect manner. Because of the signal amplification of the photoreceptor to bipolar cell synapse (Ashmore and Copenhagen, 1980), HC feedback onto cone terminals might have a larger effect on the b-wave amplitude than feedforward input onto ON-bipolar cells. Thus, it is likely that the decrease in b-wave amplitude observed here results from HC-mediated modulation of synaptic transmission from cones to ON-bipolar cells.

Our data demonstrate that FMRFamide decelerates release while $PSEM^{89S}$ accelerates release from cones, and yet both agonists decreased the amplitude of the b-wave, a seemingly

counterintuitive result. However, this finding is consistent with our understanding of the mechanism of modulation of release by horizontal cell membrane potential: The relationship between photoreceptor terminal voltage and I_{Ca2+} activation can be expressed using a Boltzmann function, with the steepest portion of the curve ideally located at the dark potential of the photoreceptor, such that small hyperpolarizations of the cone terminal dramatically decrease Ca^{2+} channel activation and therefore reduce transmitter release. Hyperpolarization of HC membrane potential with extrinsic current or light annuli shifts I_{Ca2+} such that activation increases at more negative photoreceptor voltages, thereby contributing to restoration of transmitter release from photoreceptors during maintained illumination (Verweij et al., 1996; Hirasawa and Kaneko 2003; Cadetti and Thoreson, 2006; Thoreson et al., 2008). Chemogenetic manipulation of HC membrane potential in either direction would be expected to shift the cone Ca^{2+} activation curve away from the steepest portion of the relationship, resulting in smaller changes in transmitter release in response to light-evoked hyperpolarization of cone membrane potential. The decrease in b-wave amplitude that we observe here supports this hypothesis. This finding is consistent with the idea that the set point of retinal horizontal cells, in the absence of chemogenetic perturbation, is situated to produce the maximal effect of light on cone transmitter release.

The effects of chemogenetic manipulation are consistent with perturbation of negative feedback, which is dependent exclusively on changes in HC membrane potential (Warren et al., 2016) and inconsistent with effects on positive feedback, which are triggered by influx of Ca^{2+} through Ca^{2+}-permeant AMPA receptors (Jackman et al., 2011). In the presence of AMPA stimulation, chemogenetic modulation of HC voltage was ineffective at altering transmitter release rates (Fig 2); consistent with the idea that changing HC membrane potential would have only modest effects on the driving force for Ca^{2+} influx through Ca^{2+}-permeant AMPA receptors. Thus, positive and negative feedback appear to be regulated through entirely separable and independent mechanisms.

In addition to reducing the b-wave, application of either FMRFamide or $PSEM^{89S}$ to retinas expressing their cognate receptors flattened the center surround response curve of downstream RGCs, and decreased the Lateral Inhibition Ratio. These chemogenetic interventions affected the center surround response in a similar manner to that seen when protons are buffered with HEPES (Davenport et al., 2008; Crook et al., 2009). This is consistent with the idea that uniform biasing of HC membrane potential across the retina with FMRFamide and $PSEM^{89S}$ removes local differences in inhibitory feedback at the border of the light stimulus that are essential for generating surrounds in the inner retina.

For these experiments we measured the response of RGCs before and after drug application, however, we did not classify the RGC type of each recorded cell. Using morphologic and functional experiments there are estimated 36 or more RGC types in the retina, and this is in

addition to displaced amacrine cells present within the ganglion cell-layer (Baden et al., 2016). Therefore, one could anticipate that chemogenetic perturbation of HCs may elicit a different response effect on different types of RGCs. This is further supported by experiments showing that perturbing HCs using PSEM^{89S} in retinas with HC-expressed PSAM-GlyR has different effects on the kinetics of different RGC types (Drinnenberg et al., 2018). Interpretation of these results is further complicated by the understanding that there are 3 known types of HCs (Connaughton et al., 2004), which were targeted without discrimination. Development of zebrafish lines in which either FaNaC or PSAM-GlyR is selectively expressed in specific HC subtypes would provide a powerful tool for dissecting the relative importance of each HC for generation of antagonistic surrounds in downstream RGCs.

In summary, we show a method that allows direct perturbation of HC cell membrane potential to investigate the effects that HCs have on complex retinal responses to light. While perturbing HC membrane potential cannot overcome the Ca^{2+} drive for cone synaptic release shifting of the membrane potential by depolarizing it or by restricting its depolarization greatly decreases the downstream retinal responses to a light stimulus. The use of the chemogenetic tools we present, with or without targeting to specific HC types, could therefore be further utilized to explore the direct effects that HCs have on specific types of ganglion cells, and on visual function- including color and contrast sensitivity.

ACKNOWLEDGEMENTS:
We thank Marteen Kamermans (Netherlands Institute for Neuroscience), Timothy Dunn (Duke University), and Florian Engert (Harvard University) for providing plasmids.
This work was supported by the National Institutes of Health (grant numbers R01 EY024334 and P30 EY003176).

AUTHOR CONTRIBUTION:
BBC, LCH and RHK Designed Research; BBC and LCH Performed Research, LCH Contributed unpublished tools, BBC and LCH Analyzed data, BBC, SN and RHK Wrote the paper.

DECLARATION OF INTERESTS

The authors declare no competing interests

REFERENCES

Ashmore JF, Copenhagen DR (1980) Different postsynaptic events in two types of retinal bipolar cell. Nature 288:84-86.

Atasoy D, Sternson SM (2018) Chemogenetic Tools for Causal Cellular and Neuronal Biology. Physiological reviews 98:391-418.

Baden T, Berens P, Franke K, Roman Roson M, Bethge M, Euler T (2016) The functional diversity of retinal ganglion cells in the mouse. Nature 529:345-350.

Beckwith-Cohen B, Holzhausen LC, Wang TM, Rajappa R, Kramer RH (2019) Localizing Proton-Mediated Inhibitory Feedback at the Retinal Horizontal Cell-Cone Synapse with Genetically-Encoded pH Probes. The Journal of neuroscience : the official journal of the Society for Neuroscience 39:651-662.

Betz WJ, Bewick GS (1992) Optical analysis of synaptic vesicle recycling at the frog neuromuscular junction. Science (New York, NY) 255:200-203.

Cadetti L, Thoreson WB (2006) Feedback effects of horizontal cell membrane potential on cone calcium currents studied with simultaneous recordings. Journal of neurophysiology 95:1992-1995.

Cammack JN, Schwartz EA (1993) Ions required for the electrogenic transport of GABA by horizontal cells of the catfish retina. The Journal of physiology 472:81-102.

Cassar S, Breidenbach L, Olson A, Huang X, Britton H, Woody C, Sancheti P, Stolarik D, Wicke K, Hempel K, LeRoy B (2017) Measuring drug absorption improves interpretation of behavioral responses in a larval zebrafish locomotor assay for predicting seizure liability. Journal of pharmacological and toxicological methods 88:56-63.

Choi SY, Borghuis BG, Rea R, Levitan ES, Sterling P, Kramer RH (2005) Encoding light intensity by the cone photoreceptor synapse. Neuron 48:555-562.

Connaughton VP, Graham D, Nelson R (2004) Identification and morphological classification of horizontal, bipolar, and amacrine cells within the zebrafish retina. The Journal of comparative neurology 477:371-385.

Crook JD, Davenport CM, Peterson BB, Packer OS, Detwiler PB, Dacey DM (2009) Parallel ON and OFF Cone Bipolar Inputs Establish Spatially Coextensive Receptive Field Structure of Blue-Yellow Ganglion Cells in Primate Retina. The Journal of Neuroscience 29:8372-8387.

Davenport CM, Detwiler PB, Dacey DM (2008) Effects of pH buffering on horizontal and ganglion cell light responses in primate retina: evidence for the proton hypothesis of surround formation. The Journal of neuroscience : the official journal of the Society for Neuroscience 28:456-464.

Djamgoz MB, Laming PJ (1987) Micro-electrode measurements and functional aspects of chloride activity in cyprinid fish retina: extracellular activity and intracellular activities of L- and C-type horizontal cells. Vision research 27:1481-1489.

Dong CJ, Picaud SA, Werblin FS (1994) GABA transporters and GABAC-like receptors on catfish cone- but not rod-driven horizontal cells. The Journal of neuroscience : the official journal of the Society for Neuroscience 14:2648-2658.

Dreosti E, Odermatt B, Dorostkar MM, Lagnado L (2009) A genetically encoded reporter of synaptic activity in vivo. Nature methods 6:883-889.

Drinnenberg A, Franke F, Morikawa RK, Juttner J, Hillier D, Hantz P, Hierlemann A, Azeredo da Silveira R, Roska B (2018) How Diverse Retinal Functions Arise from Feedback at the First Visual Synapse. Neuron 99:117-134.e111.

Evers HU, Gouras P (1986) Three cone mechanisms in the primate electroretinogram: two with, one without off-center bipolar responses. Vision research 26:245-254.

Firestein S, Werblin F (1989) Odor-induced membrane currents in vertebrate-olfactory receptor neurons. Science (New York, NY) 244:79-82.

Gilbertson TA, Borges S, Wilson M (1991) The effects of glycine and GABA on isolated horizontal cells from the salamander retina. Journal of neurophysiology 66:2002-2013.

Golubovic A, Kuhn A, Williamson M, Kalbacher H, Holstein TW, Grimmelikhuijzen CJ, Grunder S (2007) A peptide-gated ion channel from the freshwater polyp Hydra. The Journal of biological chemistry 282:35098-35103.

Grove JCR, Hirano AA, de los Santos J, McHugh CF, Purohit S, Field GD, Brecha NC, Barnes S (2019) Novel hybrid action of GABA mediates inhibitory feedback in the mammalian retina. PLoS biology 17:e3000200.

Hirasawa H, Kaneko A (2003) pH Changes in the Invaginating Synaptic Cleft Mediate Feedback from Horizontal Cells to Cone Photoreceptors by Modulating Ca2+ Channels. The Journal of general physiology 122:657-671.

Jackman SL, Babai N, Chambers JJ, Thoreson WB, Kramer RH (2011) A positive feedback synapse from retinal horizontal cells to cone photoreceptors. PLoS biology 9:e1001057.

Kamermans M, Werblin F (1992) GABA-mediated positive autofeedback loop controls horizontal cell kinetics in tiger salamander retina. The Journal of neuroscience : the official journal of the Society for Neuroscience 12:2451-2463.

Kay AR, Alfonso A, Alford S, Cline HT, Holgado AM, Sakmann B, Snitsarev VA, Stricker TP, Takahashi M, Wu LG (1999) Imaging synaptic activity in intact brain and slices with FM1-43 in C. elegans, lamprey, and rat. Neuron 24:809-817.

Klaassen LJ, Sun Z, Steijaert MN, Bolte P, Fahrenfort I, Sjoerdsma T, Klooster J, Claassen Y, Shields CR, Ten Eikelder HM, Janssen-Bienhold U, Zoidl G, McMahon DG, Kamermans M (2011) Synaptic transmission from horizontal cells to cones is impaired by loss of connexin hemichannels. PLoS biology 9:e1001107.

Koizumi A, Zeck G, Ben Y, Masland RH, Jakobs TC (2007) Organotypic culture of physiologically functional adult mammalian retinas. PloS one 2:e221.

Kramer RH, Davenport CM (2015) Lateral Inhibition in the Vertebrate Retina: The Case of the Missing Neurotransmitter. PLoS biology 13:e1002322.

Krause S, Schwarz W (2005) Identification and selective inhibition of the channel mode of the neuronal GABA transporter 1. Mol Pharmacol 68:1728-1735.

Kreitzer MA, Andersen KA, Malchow RP (2003) Glutamate modulation of GABA transport in retinal horizontal cells of the skate. The Journal of physiology 546:717-731.

Kyrozis A, Reichling DB (1995) Perforated-patch recording with gramicidin avoids artifactual changes in intracellular chloride concentration. Journal of neuroscience methods 57:27-35.

Magnus CJ, Lee PH, Atasoy D, Su HH, Looger LL, Sternson SM (2011) Chemical and genetic engineering of selective ion channel-ligand interactions. Science (New York, NY) 333:1292-1296.

Malchow RP, Ripps H (1990) Effects of gamma-aminobutyric acid on skate retinal horizontal cells: evidence for an electrogenic uptake mechanism. Proc Natl Acad Sci U S A 87:8945-8949.

Miller RF, Dacheux RF (1983) Intracellular chloride in retinal neurons: measurement and meaning. Vision research 23:399-411.

Nelson R, Bender AM, Connaughton VP (2008) Transporter-mediated GABA responses in horizontal and bipolar cells of zebrafish retina. Visual neuroscience 25:155-165.

Niklaus S, Neuhauss SCF (2017) Genetic approaches to retinal research in zebrafish. Journal of neurogenetics 31:70-87.

Paik S-S, Park N-G, Lee S-J, Han H-K, Jung C-S, Bai S-H, Chun M-H (2003) GABA receptors on horizontal cells in the goldfish retina. Vision research 43:2101-2106.

Rea R, Li J, Dharia A, Levitan ES, Sterling P, Kramer RH (2004) Streamlined synaptic vesicle cycle in cone photoreceptor terminals. Neuron 41:755-766.

Robson JG, Frishman LJ (1995) Response linearity and kinetics of the cat retina: the bipolar cell component of the dark-adapted electroretinogram. Visual neuroscience 12:837-850.

Saszik S, Bilotta J, Givin CM (1999) ERG assessment of zebrafish retinal development. Visual neuroscience 16:881-888.

Saszik S, Alexander A, Lawrence T, Bilotta J (2002) APB differentially affects the cone contributions to the zebrafish ERG. Visual neuroscience 19:521-529.

Schanuel SM, Bell KA, Henderson SC, McQuiston AR (2008) Heterologous expression of the invertebrate FMRFamide-gated sodium channel as a mechanism to selectively activate mammalian neurons. Neuroscience 155:374-386.

Seeliger MW, Rilk A, Neuhauss SC (2002) Ganzfeld ERG in zebrafish larvae. Documenta ophthalmologica Advances in ophthalmology 104:57-68.

Shields CR, Klooster J, Claassen Y, Ul-Hussain M, Zoidl G, Dermietzel R, Kamermans M (2007) Retinal horizontal cell-specific promoter activity and protein expression of zebrafish connexin 52.6 and connexin 55.5. The Journal of comparative neurology 501:765-779.

Stockton RA, Slaughter MM (1989) B-wave of the electroretinogram. A reflection of ON bipolar cell activity. The Journal of general physiology 93:101-122.

Takahashi K, Miyoshi S, Kaneko A (1995) GABA-induced chloride current in catfish horizontal cells mediated by non-GABAA receptor channels. The Japanese journal of physiology 45:437-456.

Thoreson WB, Miller RF (1994) Actions of (1S,3R)-1-aminocyclopentane-1,3-dicarboxylic acid (1S,3R-ACPD) in retinal ON bipolar cells indicate that it is an agonist at L-AP4 receptors. The Journal of general physiology 103:1019-1034.

Thoreson WB, Mangel SC (2012) Lateral interactions in the outer retina. Progress in retinal and eye research 31:407-441.

Thoreson WB, Babai N, Bartoletti TM (2008) Feedback from Horizontal Cells to Rod Photoreceptors in Vertebrate Retina. The Journal of Neuroscience 28:5691-5695.

Verweij J, Kamermans M, Spekreijse H (1996) Horizontal cells feed back to cones by shifting the cone calcium-current activation range. Vision research 36:3943-3953.

Vessey JP, Stratis AK, Daniels BA, Da Silva N, Jonz MG, Lalonde MR, Baldridge WH, Barnes S (2005) Proton-mediated feedback inhibition of presynaptic calcium channels at the cone photoreceptor synapse. J Neurosci 25:4108-4117.

Wang TM, Holzhausen LC, Kramer RH (2014) Imaging an optogenetic pH sensor reveals that protons mediate lateral inhibition in the retina. Nature neuroscience 17:262-268.

Warren TJ, Van Hook MJ, Tranchina D, Thoreson WB (2016) Kinetics of Inhibitory Feedback from Horizontal Cells to Photoreceptors: Implications for an Ephaptic Mechanism. The Journal of neuroscience : the official journal of the Society for Neuroscience 36:10075-10088.

Williams PR, Morgan JL, Kerschensteiner D, Wong RO (2013) In vivo imaging of zebrafish retina. Cold Spring Harbor protocols 2013.

Chapter 3: Transitional section

In Chapter 2 of this dissertation, we established 2 chemogenetic tools, PSAM-GlyR and FaNaC, to directly manipulate the membrane potential of HCs in the zebrafish retina and exhibited the successful expression of these transgenic receptors both ex-vivo and in-vivo. Prior to evaluating the effects that activation of PSAM-GlyR and FaNaC have on retinal function we established the resting potential of HCs in zebrafish and quantified the effects that PSAM-GlyR and FaNaC have on the HC membrane potential (i.e., degree of hyperpolarization and depolarization, respectively). After showing that FaNaC activation induces a depolarization of HCs and that PSAM-GlyR induces HC hyperpolarization, we explored the effects that HC hyperpolarization and depolarization have on upstream and downstream retinal function.

We were able to show that chemogenetic activation of HCs alters vesicular cone release causing decreased FM1-43 dye loss with FMRFamide activation of FaNaC, and increased dye loss with $PSEM^{89S}$ activation of PSAM-GlyR. In both cases, addition of AMPA dominated synaptic release causing a profound increase in dye loss, which was not significantly affected by the addition of either FMRFamide or $PSEM^{89S}$. This indicated that while our chemogenetic tools affect the negative feedback driven by HCs, they are insufficient to overcome signals of HC positive feedback which regulate Ca^{2+} dependent exocytosis in photoreceptors.

While the evaluation of the effects of FaNaC activation on dissociated HCs was rather straight forward, explaining the effect of $PSEM^{89S}$ on HC membrane potential and feedback control of cone release proved to be challenging. Historically, the value of E_{Cl-} in HCs has been ambiguous. Previous studies employing different recording methods estimated E_{Cl-} values ranging from -50 mV, when using a voltage-indicator dye on enzymatically dissociated HCs (Nelson et al., 2008), to -17 mV when measured using sharp electrodes on HCs in situ (Miller and Dacheaux, 1983). However, E_{Cl-} is easily perturbed when electrodes are used. Because the pipette volume is much larger than the cytoplasmic volume, at equilibrium E_{Cl-} should be determined by the Cl^- concentration in the pipette. In the voltage-indicator dye experiments (Nelson et al., 2008) HC membrane potential could be manipulated with the ionophore gramicidin, a non-selective cation channel. Gramicidin is impermeant to Cl^-, thus preserving the normal internal Cl^- concentration (Kyrozis and Reichling, 1995). The small acceleration of FM1- 43 release that we observed upon application of $PSEM^{89S}$ to PSAM-GlyR retina supported the hyperpolarization of the membrane potential, consistent with E_{Cl-} being slightly more hyperpolarized than rest. Direct evidence for this was obtained using the perforated patch recording technique, and the membrane potential documented by us was similar to that noted previously (Nelson et al., 2008).

When looking at the effect that HC membrane potential perturbation had on downstream retinal function (i.e., bipolar cells and RGCs) we noticed that a reduction in b-wave and perturbation of center-surround signaling occurred with both hyperpolarization and depolarization of HCs. This could be explained by the Boltzmann distribution function, with the membrane potential of HCs ideally set at the dark current, such that slight perturbations of this set point impair the ability of the HCs to responds at their maximal potential to changes in light stimuli.

With these findings we chose to further explore the effect that HC perturbation has on lateral inhibition in the inner retina, and were set to identify the location of the proton mediated signal that regulates lateral inhibition in the outer retina. For this purpose, 3 transgenic zebrafish were utilized, each expressing a pHluorin to detect changes in pH in various locations in the HC-cone photoreceptor synapse. Two phluorins were expressed on the photoreceptor side- CalipHluorin which is restricted to a small area near the voltage gated Ca^{2+} channel and the ribbon synapse and synaptopHluorin, which is more widely dispersed on the cone photoreceptor synaptic membrane. The third pHluorin was expressed on the HC side of the synapse. Lastly, fish expressing synaptopHluorin were crossed with our FaNaC fish, which were presented in Chapter 2, and the effect of HC depolarization on pH in the synaptic cleft was inspected. Results of these findings are detailed in Chapter 4.

Chapter 4: **Localizing proton-mediated inhibitory feedback at the retinal horizontal cell-cone synapse with genetically-encoded pH probes**

Published in the Journal of Neuroscience in January 2019

Billie Beckwith-Cohen[1], Lars C. Holzhausen[2], Tzu-Ming Wang[2], Rajit Rajappa[2] and Richard H. Kramer[1,2]*

[1]Vision Science Graduate Program, University of California, Berkeley

[1,2]Department of Molecular and Cell Biology, University of California, Berkeley

Citation:

Beckwith-Cohen B, Holzhausen LC, Wang TM, Rajappa R, Kramer RH. Localizing Proton-Mediated Inhibitory Feedback at the Retinal Horizontal Cell-Cone Synapse with Genetically-Encoded pH Probes. J Neurosci. 2019 Jan 23;39(4):651-662. doi: 10.1523/JNEUROSCI.1541-18.2018. Epub 2018 Nov 30. PMID: 30504272; PMCID: PMC6343651.

ABSTRACT

Lateral inhibition in the vertebrate retina depends on a negative feedback synapse between horizontal cells (HCs) and rod and cone photoreceptors. A change in pH is thought to be the signal for negative feedback, but its spatial profile in the synaptic cleft is unknown. Here we use 3 different membrane proteins, each fused to the same genetically-encoded pH-sensitive GFP (pHluorin), to probe synaptic pH in retina from transgenic zebrafish (*Danio rerio*) of either sex. We used the cone transducin promoter to express SynaptopHluorin (pHluorin on VAMP2) or CalipHluorin (pHluorin on an L-type Ca^{2+} channel) and the HC-specific connexin-55.5 promoter to express AMPApHluorin (pHluorin on an AMPA receptor). Stimulus light led to increased fluorescence of all three probes, consistent with alkalinization of the synaptic cleft. The receptive field size, sensitivity to surround illumination, and response to activation of an alien receptor expressed exclusively in HCs, are consistent with lateral inhibition as the trigger for alkalinization. However, SynaptopHluorin and AMPApHluorin, which are displaced farther from cone synaptic ribbons than CalipHlourin, reported a smaller pH change. Hence, unlike feed-forward glutamatergic transmission, which spills over to allow cross-talk between terminals in the cone network, the pH change underlying HC feedback is compartmentalized to individual synaptic invaginations within a cone terminal, consistent with private line communication.

SIGNIFICANCE STATEMENT

Lateral inhibition (LI) is a fundamental feature of information processing in sensory systems, enhancing contrast sensitivity and enabling edge discrimination. Horizontal cells (HCs) are the first cellular substrate of LI in the vertebrate retina, but the synaptic mechanisms underlying LI are not completely understood, despite decades of study. This paper makes a significant contribution to our understanding of LI, by showing that each HC-cone synapse is a "private-line" that operates independently from other HC-cone connections. Using transgenic zebrafish expressing pHluorin, a pH-sensitive GFP variant spliced onto 3 different protein platforms expressed either in cones or HCs we show that the feed-back pH signal is constrained to individual cone terminals, and more stringently, to individual synaptic contact sites within each terminal.

INTRODUCTION

Retinal horizontal cells (HCs) receive synaptic input from rod and cone photoreceptors, but they also send signals back to the photoreceptors to regulate release of their neurotransmitter, glutamate (Wu, 1991). HC feedback is crucial for lateral inhibition, a retinal circuit mechanism for enhancing contrast sensitivity (Campbell and Robson, 1968) and color discrimination (Tomita, 1965). Lateral inhibition at the first synapse in the retina sets the stage for antagonistic center-surround receptive fields exhibited throughout the visual system, an organizational feature that is essential for high acuity vision.

Several different chemical and electrical signals have been proposed as mediators of HC feedback (Kramer and Davenport, 2015). Identification of the feedback signal has been complicated by the reciprocal nature of the synapse and its inaccessibility because it occurs in an invagination, deep within the terminals of cones. The first proposed feedback signal was the inhibitory neurotransmitter GABA, which is synthesized and released by HCs (Schwartz, 1982). However, pharmacological blockers of GABA receptors fail to reduce HC feedback (Thoreson and Burkhardt, 1990; Verweij et al., 1996) and have no significant effect on the downstream consequences of HC-mediated lateral inhibition (Davenport et al., 2008), inconsistent with GABA serving as the HC feedback signal. Second, an electrical field effect, known as ephaptic transmission, has been proposed as an HC feedback mechanism (Byzov and Shura-Bura, 1986; Kamermans et al., 2001). The tips of HC dendrites have a high density of ion channels directly opposed to synaptic ribbons in cone terminals. Current is thought to flow through these channels and across the extracellular resistance, causing a voltage drop that is sensed by the cone voltage-gated Ca^{2+} channels, thereby altering Ca^{2+}-dependent glutamate release (Verweij et al., 1996). HC to cone feedback exhibits a brief, but measurable synaptic delay, which may be inconsistent with an instantaneous ephaptic mechanism (Warren et al., 2016a), although the interpretation of these results has been debated (Chapot et al., 2017; Cenedese et al., 2017). Third, an HC-driven change in proton concentration has been proposed to serve as the HC feedback signal (Hirasawa and Kaneko, 2003; Vessey et al., 2005). In this scenario, the voltage-dependent gating of L-type Ca^{2+} channels in cones is regulated by protonation of a site in the channel protein, again altering Ca^{2+}-dependent glutamate release.

Most of the evidence, pro or con, about each of the three proposed signals has involved genetic or pharmacological manipulations intended to block or mimic signal transduction. By contrast, demonstrating whether a putative signal is actually present at the synapse, at a level sufficient to account for feedback inhibition, has been more challenging. The one exception is pH. The development of pHluorin, a genetically-encoded protein probe for pH, circumvents the inaccessibility problem by allowing local optical measurement of pH, providing a direct test of the pH hypothesis. In a previous study (Wang et al., 2014), we developed the novel fluorescent probe CalipHluorin, in which pHluorin was spliced onto the extracellular side of the accessory

$\alpha_2\delta_4$ subunit of the L-type Ca^{2+} channel. CalipHluorin was particularly well situated as a probe because L-type channels are the relevant targets for HC-feedback in cones (Verweij et al., 1996; Cadetti and Thoreson, 2006). Here, to learn about the spatial profile of the proton signal and determine whether it spills over to adjacent synapses, we use two additional protein platforms for pHluorin, and exploit the advantages of zebrafish genetics to display these probes in a cell-type specific manner.

MATERIALS AND METHODS

Transgenic fish

Transgenic fish expressing CalipHluorin (ZFIN ID: ZDB-FISH-150901-12656) and/or FaNaC (ZFIN ID: ZDB-FISH-150901-9090) were engineered previously (Wang et al., 2014). SynpatopHluorin fish (ZFIN ID: ZDB-FISH-150901-24914; Holzhausen et al., 2009) were kindly donated by S. Brockerhoff, University of Washington. AMPApHluorin fish (ZFIN ID: ZDB-FISH-181031-4) were generated specifically for this project. The rat GluR2 subunit of the AMPA receptor was generously provided by R. Huganir, Johns Hopkins University School of Medicine. A tandem sequence containing the superecliptic pHluorin, a protease recognition site and a 15-residue linker was inserted between the predicted signal peptide and the coding sequence of the GluR2 subunit. The resulting construct was cloned into vector pDONR221 (Invitrogen) to produce pME-AMPApHluorin. Gateway recombination cloning (Invitrogen) with p5E- Cx55.5 (Shields et al., 2007) (kindly provided by M. Kamermans, Netherlands Institute for Neuroscience), pME-AMPApHluorin, and p3E-MTpA and pDestTol2CG2 from the Tol2kit (Kwan et al. 2007) was used for generating the AMPApHluorin construct. One- or two-cell-stage zebrafish (*Danio rerio,* AB strain) embryos were microinjected with the construct together with Tol2 mRNA for a higher germline transmission rate (Kwan et al., 2007). The transgene-positive F0 founders were selected by screening for green heart fluorescence in embryos at 2–4 days post fertilization (Kwan et al., 2007) and raised at 28.5 °C in a 14 h light, 10 h dark cycle. The adult F0 fish were inbred, and their transgene-positive progeny were screened by green heart fluorescence, raised, and used for imaging experiments and immunohistochemistry.

To generate SynaptopHluorin and FaNaC double transgenic fish, the SynaptopHluorin transgenic fish line was crossed with the FaNaC fish line. Embryos and larvae were treated with phenylthiourea (PTU) to prevent pigmentation and phenotypically screen for both transgenes at dpf4. For SynaptopHluorin the expression of pHluorin (GFP) was identified in the cone layer in larval eyes (thus necessitating the use of PTU. FaNaC was identified by positive green heart fluorescence.

Tissue preparation

Adult zebrafish (*Danio rerio)* of either sex were used in all experiments. Procedures, animal care and use were approved by the University of California, Berkeley Animal Care and Use Committee. Fish were dark adapted for >30 minutes, and euthanized by immersion in

400mg/L MS-222, followed by decapitation. Retinas were removed from retinal pigment epithelium under infrared light. For immunohistochemistry eyes were fixed in 4% paraformaldehyde, rinsed in PBS, and immersed for 1 hour in 15% sucrose followed by 1 hour in 30% sucrose for cryoprotection. The eyes were embedded in tissue-freezing medium (General Data Company Inc.), flash-frozen over dry ice, and kept in -80° C until use. Eyes were sliced to 14 µm in thickness using a microtome (Thermo Fisher Microm HM550) and kept in -20° C until immunohistochemistry was performed.

Solutions

Unless specified otherwise, retinas were continuously perfused with bicarbonate-buffered saline solution containing (in mM) 100 NaCl, 2.5 KCl, 1 $MgCl_2$, 1 $CaCl_2$, 0.4 ascorbic acid, 20 dextrose and 25 $NaHCO_3$ bubbled with 5% CO_2 and 95% O_2, pH=7.3. For the pH experiments on rat hippocampal cells, the solution contained (in mM) 115 NaCl, 2.5 KCl, 1 $MgCl_2$, 1 $CaCl_2$ and 20 dextrose as well as with 20 mM of one of the following buffers: 2-(*N*-morpholino) ethanesulfonic acid (MES) for pH 5.5 and HEPES for pH 7.4. Light-response experiment buffers contained the same solution as that used in pH experiments with the addition of 0.4 mM ascorbic acid and 20 mM HEPES. pH titration solutions (Fig. 1C) contained (in mM): MES buffer – 150 NaCl, 4 KCl, 2 CaCl2, 1 MgCl2, 10 Glucose & 10 MES; HEPES buffer – 150 NaCl, 4 KCl, 2 CaCl2, 1 MgCl2, 10 Glucose & 10 HEPES.

Immunohistochemistry and antibodies

Protein blocking solution used for immunohistochemistry included 34.5ml of PBS, 0.5ml Triton x-100 (Sigma Aldrich) diluted to 10x in PBS and 15ml bovine serum albumin fraction V (1g/100ml) (MP Biomedicals LLC, Cat# 160069), chilled to 4° C. Additional blocking was achieved using unconjugated secondary antibodies. Tissue sections were rinsed on a shaker in chilled PBS for three 5-minute cycles at 100 rpm, with fresh PBS used for each cycle. Sections were immersed in chilled blocking solution including goat anti-mouse (Thermo Fisher Scientific Cat# A16080, RRID:AB_2534754) and donkey anti-rabbit unconjugated igG (Thermo Fisher Scientific Cat# 31238, RRID:AB_429690) antibodies at a 1:1000 dilution and placed on a shaker for 1 hour at 100 rpm. The sections were rinsed on a shaker in chilled PBS for three 5 minute cycles at 100 rpm. The sections were immersed by placing 200 µl fresh blocking solution including mouse anti-GFP monoclonal unconjugated antibody (Abcam Cat# ab1218, RRID:AB_298911) and rabbit IgG anti-CtBp2 (RIBEYE labeling, Thermo Fisher Scientific Cat# PA5-30001, RRID:AB_2547475) polyclonal unconjugated antibody, both at a 1:400 dilution. Sections were covered using a gasket and placed on a shaker at 100 rpm in a 4° C cold room for 36-48 hours. Negative controls included sections of the same tissue whilst omitting the primary antibodies. The sections were rinsed on a shaker in chilled PBS for three 5 minute cycles at 100 rpm and immersed in blocking solution including Alexa 488 goat anti-mouse igG (Thermo Fisher Scientific Cat# A-11001, RRID:AB_2534069) and Alexa-647 donkey anti-rabbit IgG (Thermo Fisher Scientific Cat# A-31573, RRID:AB_2536183) antibodies at 1:1000 dilution. The sections

were placed on a shaker for 1 hour, the rinsed for 3 cycles, air dried and sealed using Fluoromount-G with DAPI mounting solution (Invitrogen).

HEK293T cell pHluorin titration:

HEK293T cells grown on 18mm coverslips coated with Poly-lysine (Sigma-Aldrich) were transfected one day after plating with 2µg/well CalipHluorin or AMPApHluorin plasmids. A day after transfection, pHluorin imaging was performed on a confocal Carl Zeiss LSM780 microscope while perfusing with solutions of a pH ranging from 5.0–8.0. MES based buffer was used to prepare solutions for pH 5–6.5 and HEPES based buffer was used to prepare solutions with a pH of 7–8.

Image acquisition

Flat-mounted retinae were transferred to an imaging chamber with the photoreceptor side facing the bottom of the chamber. We used a custom-built 2-photon microscope as described previously (Wang et al., 2014). The microscope was controlled by ScanImage r3.6 software (Pologruto et al., 2003) with in-house developed plugins. For light stimulation experiments, an area 30 × 30 μm^2 was imaged at a frame rate of 128 ms per frame and binned into 64- × 64-pixel images. Immunohistochemistry- for super resolution experiments we used a confocal Carl Zeiss LSM880 microscope equipped with Airyscan set to super resolution mode. Alexa Fluor 488 and 647 were excited at 488 nm and 633nm using Argon and HeNe lasers respectively; DAPI was excited using a Diode 405nm laser.

Light stimulation

Light stimulation was performed as previously described (Wang et al., 2014). Briefly, light sources were a LUXEON Rebel Blue light-emitting diode (LED) (PHILIPS) shortpass filtered at 460 nm and a LUXEON Rebel Amber LED longpass filtered at 550 nm. Light from the two LEDs was combined with a 505-nm longpass dichroic mirror and coupled to the projection optics with an optical fiber. The green portion of the spectrum (460–550 nm) was filtered out to protect the photomultiplier from photodamage. We used a light intensity of 10^{18}–10^{19} photons m^{-2} s^{-1} (Davenport et al., 2008) measured with a photometer at the specimen plane. A pattern mask (e.g., spot or annulus) was placed in the projection light and projected onto retinae through the condenser. A program written in MATLAB (MathWorks) was used to command the shutter (TS6B, UNIBLITZ) for controlling flash duration. A flash duration of 508 ms was used. Light stimulation was given at ∼1 s after the beginning of a scan series and was repeated three times in each experimental run.

Image analysis

A region of interest (ROI) was selected from the cone-HC terminal image. The ROI was generated in ImageJ (rsbweb.nih.gov/ij) using a thresholding-based technique as previously described (Wang et al., 2014). We excluded from the ROI the first row of pixels (i.e., the first 2 ms of the scanned image), collected after terminating the light flash, to avoid detecting afterglow of the stimulation light. The background signal, measured at the end of the experiment in the absence of laser scanning, was subtracted from each image. To estimate photobleaching, the average pixel intensity within the ROI of each frame (termed *F*) was fitted with a single-exponential function $y = ae^{-bx}$, where *x* is the frame number and *y* is the intensity as previously described (Wang et al., 2014). Fluorescence intensities acquired during the light flash were excluded from the photobleach fitting routine because they were confounded with the stimulus light as previously described (Wang et al., 2014). To compensate for photobleaching, the original intensity (*F*) of each frame was divided by its corresponding value in the fitted curve (*y*). The compensated light responses from the three flashes were aligned, and the mean response was calculated and defined as *n* of 1 as previously described (Wang et al., 2014). For Figure 3D a radial intensity profile was created for each probe using ROIs generated in ImageJ around individual terminals. Image resolutions were matched and sum-projection intensity profiles were generated using a macro written for this purpose. Variations in terminal intensity were normalized and each sample was analyzed independently so that dim images carry the same weight as bright ones in the final analysis.

For Figure 1C Quantitative analysis was performed using ImageJ. Data was generated from 2 different regions in each experiment. The average normalized change in fluorescence from those regions was plotted as a function of pH. The magnitude of normalized fluorescence change as a function of pH was fitted to a simple Henderson–Hasselbach equation, $y = y0 + ymax/(1 + 10(pKa-pH))$, where y0 represents the offset, ymax the dynamic range, and pKa is the logarithm of equilibrium constant for protonation.

Electron Microscopy

Zebrafish retinae were fixed and prepared for electron microscopy using standard methods as previously described (Rea et al., 2004). Images were obtained using Advanced Microscopy Techniques (AMT) digital camera imaging systems for transmission electron microscopes (Scientex).

Experimental Design and Statistical analysis

Unless otherwise noted, sample sizes for each experimental condition represent independent frames imaged from at least 4 zebrafish retinas with the mean fluorescence of many individual terminals averaged to give a single value for each frame. Statistical significance for sample numbers less than ten was determined by using the two-sided nonparametric Mann-Whitney *U* test. Significance for multiple group comparisons was determined using one-way ANOVA followed by the two-tailed Student's *t* test. Significance was otherwise determined by

two-tailed Student's *t* test. Data points and error bars represent the mean ± s.e.m. Statistics were performed using Microsoft Office Professional Excel version 2016, IGOR Pro 8 or Matlab 9.

RESULTS

CalipHluorin, SynaptopHluorin and AMPApHluorin: three genetically-encoded pH reporters for investigating proton signaling at the HC-cone synapse

We exploited the unique subcellular distributions of key signaling proteins to explore the light-elicited proton gradient in the HC-cone synapse (Figure 1). CalipHluorin, described previously (Wang et al., 2014), was designed to detect local pH directly at the cone Ca^{2+} channels that mediate neurotransmitter release. Cone-specific expression of CalipHluorin is driven with the promoter for the cone transducin α-subunit (TaC) (Kennedy et al., 2007). Electron microscopy (Raviola and Gilula, 1975) and immunofluorescence microscopy (Mercer et al., 2011) suggest that the Ca^{2+} channels are positioned directly adjacent to synaptic ribbons in cones, which would place CalipHluorin very close to the sites of neurotransmitter release, and exactly on the relevant physiological target protein regulated by HC feedback.

SynaptopHluorin (Miesenbock et al., 1998) is pHluorin fused onto the C-terminus (luminal or extracellular side) of VAMP2 (also called synaptobrevin), a synaptic vesicle protein that is part of the SNARE complex. Cone-specific expression of VAMP2 was also driven by the TaC promoter (Holzhausen et al., 2009). SynaptopHluorin has been used as a probe of exocytosis, because it becomes fluorescent only when acidic synaptic vesicles fuse with the plasma membrane, exposing the probe to the neutral pH of the extracellular space (Miesenbock et al., 1998; Sankaranarayanan and Ryan, 2000). However, a large fraction of VAMP2 molecules escape endocytotic recapture and remain stranded on the plasma membrane where they are sensitive to extracellular pH (Sankaranarayanan and Ryan, 2000).

Finally, AMPApHluorin is pHluorin fused onto the α2-subunit of an ionotropic glutamate receptor [previously called pHluorin–GluR2; (Ashby et al., 2004)]. The connexin-55.5 promoter ensures that AMPApHluorin is expressed selectively in HCs (Shields et al., 2007).

Since the identical pHluorin variant was used in all 3 probes, the dependence of fluorescence on pH should also be identical. We verified this by perfusing various pH-buffered solutions on HEK293 cells expressing either CalipHluorin or AMPAphluorin and on retinae expressing SynaptopHluorin. The titration curves were identical, with a pKa of 7.15±0.04 for CalipHluorin, 7.22±0.08 for SynaptopHluorin and 7.23±0.10 for AMPApHluorin (Figure 1).

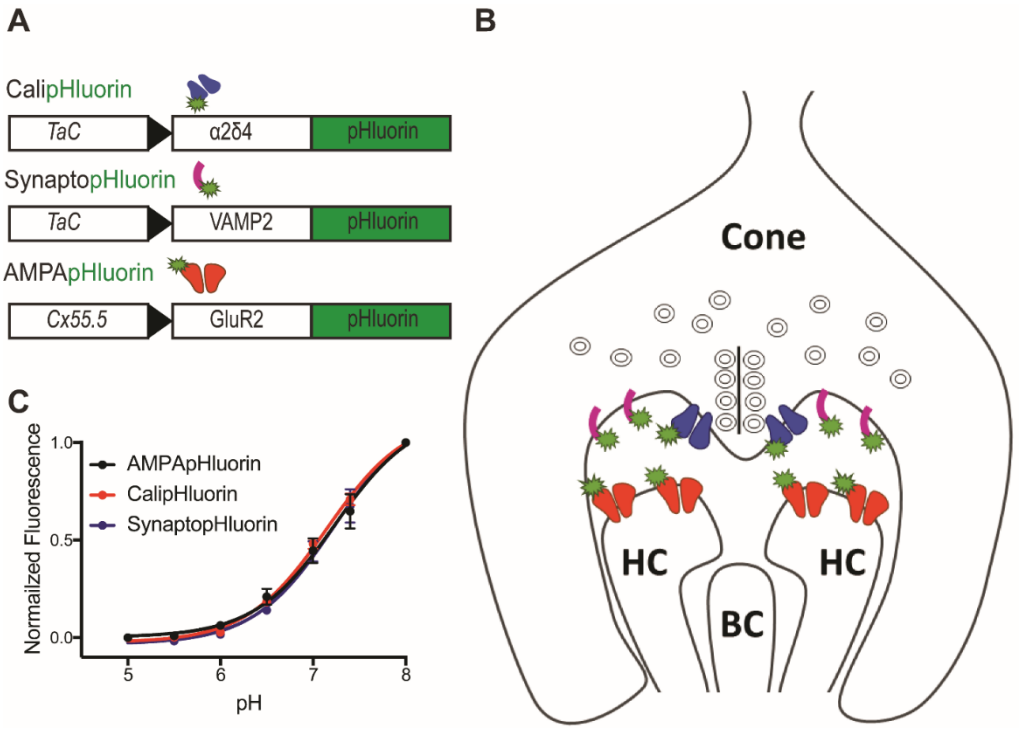

Figure 1. Three genetically encoded pH-probes for studying the HC-cone synapse.
(A) Three pHluorin constructs. CalipHluorin, driven by the TaC promoter, is pHluorin fused onto the α2δ4 subunit of the L-type Ca^{2+} channel. SynaptopHluorin, also driven by TaC, is pHluorin fused onto the SNARE protein VAMP2. AMPApHluorin is pHluorin fused onto the α2-subunit of an ionotropic glutamate receptor. (B) Proposed architecture of pHluorin within the invaginating synapse. CalipHluorin and SynaptopHluorin are on cone terminals; AMPApHluorin is on horizontal cell (HC) dendrites. A bipolar cell (BC) dendrite forms the third element of the synaptic triad. (C) The estimated pKa of pHluorin is not altered when tagged to different cellular proteins. The average normalized change in fluorescence from 3 experiments is plotted as a function of pH. The number of cells used in the averaged data was: SynaptopHluorin (n = 18); AMPApHluorin (n = 13); CalipHluorin (n = 10). The respective colored solid lines are fits to the simple Henderson–Hasselbach equation.

Distinct distributions of the pH reporters at the synapse.

We generated transgenic zebrafish lines that stably express these 3 probes, each containing the same superecliptic pHluorin variant of GFP. In the retina, the fluorescence intensity of each probe depends on two factors: the expression density of the probe and the local pH to which it is exposed. To disambiguate these factors, we first compared the expression density of each probe by immunostaining the retina with a fluorescent antibody against GFP. We used super-resolution microscopy (Zeiss Airyscan) on thin retinal slices (Figure 2) to provide images with 140-250 nm resolution, much better than possible with direct 2-photon imaging of fluorescent probes such as pHluorin >500 nm (Svoboda and Yasuda, 2006). To visualize synaptic ribbons, we used a fluorescent antibody to label RIBEYE, its main structural protein (Schmitz et al., 2000).

We found that in cone terminals, CalipHluorin was juxtaposed to the synaptic ribbons, matching the normal location of the voltage-gated Ca^{2+} channels in cones. SynaptopHluorin was more dispersed throughout the cone terminals, consistent with diffusion of VAMP2 from synaptic release sites by lateral diffusion in the plasma membrane of the terminal (Sankaranarayanan and Ryan, 2000). AMPApHluorin was present throughout the HCs, both in the cell bodies and dendrites. Some of the AMPApHluorin protein appeared in puncta, perhaps corresponding to intracellular compartments, a common consequence of over-expression.

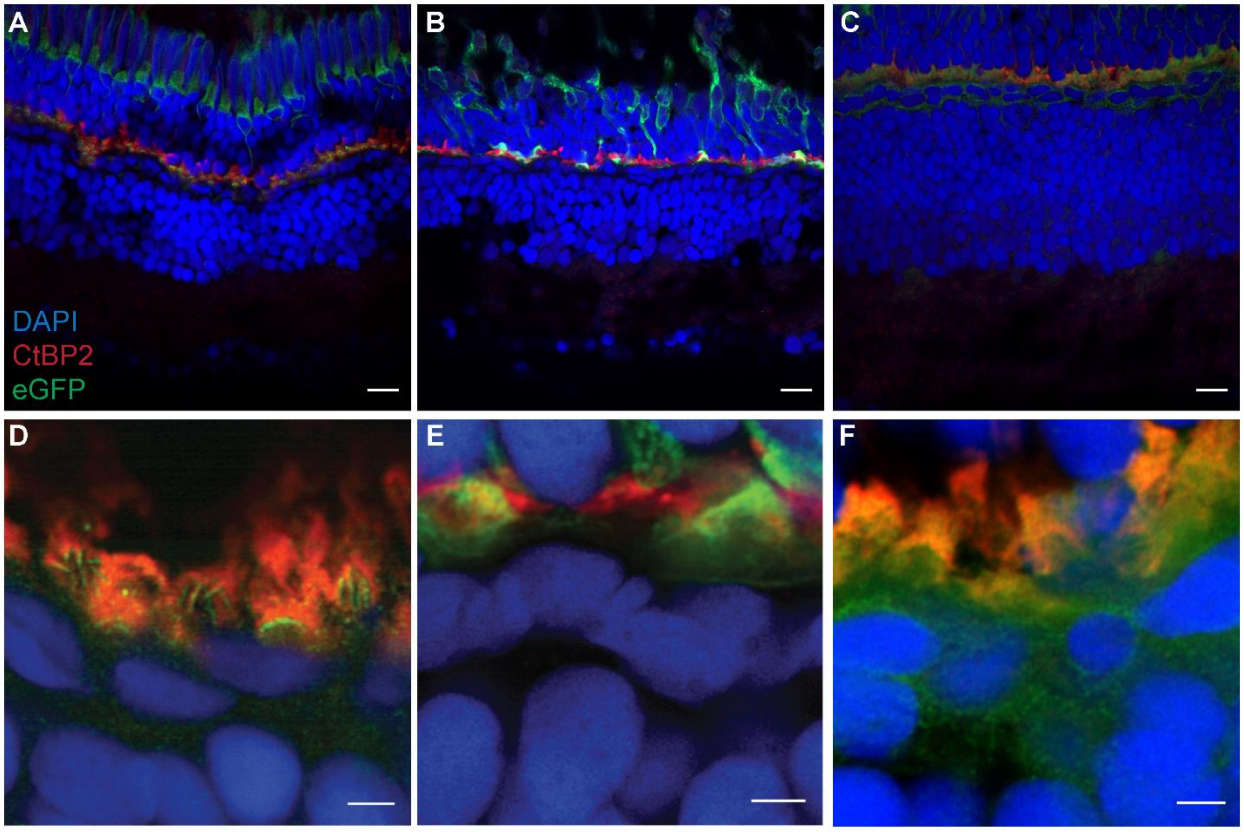

Figure 2: Immunolocalization of CalipHluorin, SynaptopHluorin and AMPApHluorin in the retina.

Antibody against GFP labels pHluorin (green), antibody against CtBP2 labels RIBEYE (red), and DAPI labels cell nuclei (blue). (A) CalipHluorin labeling is restricted to cones, including in inner segments, outer segments, and terminals. (B) SynaptopHluorin is also limited to cones, appearing in inner segments, outer segments, and terminals. (C) AMPApHluorin is limited to HCs. (D) Within the terminals, CalipHlourin is juxtaposed to synaptic ribbons, which contain RIBEYE. (E) Within the terminals, labeling of SynaptopHluorin is diffuse. (F) AMPApHluorin appears diffusely throughout horizontal cell soma and dendrites. Scale bar=10µm (A-C), Scale bar=2µm (D-F).

Next, we examined the resting pHluorin fluorescence of each of the probes in darkness; i.e. without visible wavelengths of light. Retinas were continuously imaged with 2-photon microscopy using 910 nm light. Although infrared 2-photon scanning can generate a rod light response and some degree of light adaptation (Denk and Detwiler, 1999), both should reach steady-state with continuous imaging, allowing measurement of signals elicited by a bright flash of visible light. Figure 3A shows that steady-state SynaptopHluorin and CalipHluorin fluorescence was detected throughout cones, including in outer segments and inner segments, but the signal was brightest in cone terminals. AMPApHluorin fluorescence was distributed throughout HCs, but brightest in rosettes near the periphery of the cone terminals (Figure 3B). AMPApHluorin fluorescence also appeared in isolated smaller puncta, at the tips of HC dendrites adjacent to rod terminals (Figure 3B). Similar rosettes and isolated smaller puncta have been observed in zebrafish retina stained with an antibody against the GluR2 protein (Klooster et al., 2009). Hence in the synaptic region, the distribution of steady-state pHluorin probe fluorescence coincides with the antibody labeling.

We analyzed the distribution of the fluorescence signal at HC-cone contacts by imaging hundreds of individual terminals in retinal flat mounts from zebrafish with CalipHluorin (n=486), SynaptopHluorin (n=167) or AMPApHluorin (n=320). For each probe, an average spatial profile and associated heat map were generated (Figure 3C, D). The average peak intensity was 540 nm from the terminal center for CalipHluorin, 995 nm for AMPApHluorin, and 1200 nm for SynaptopHluorin. Consistent with the immunolabeling results, we found that the intrinsic fluorescence signals from SynaptopHluorin and AMPApHluorin were maximal at the perimeter of the terminal, while CalipHluorin fluorescence was maximal closer to the center of the terminal.

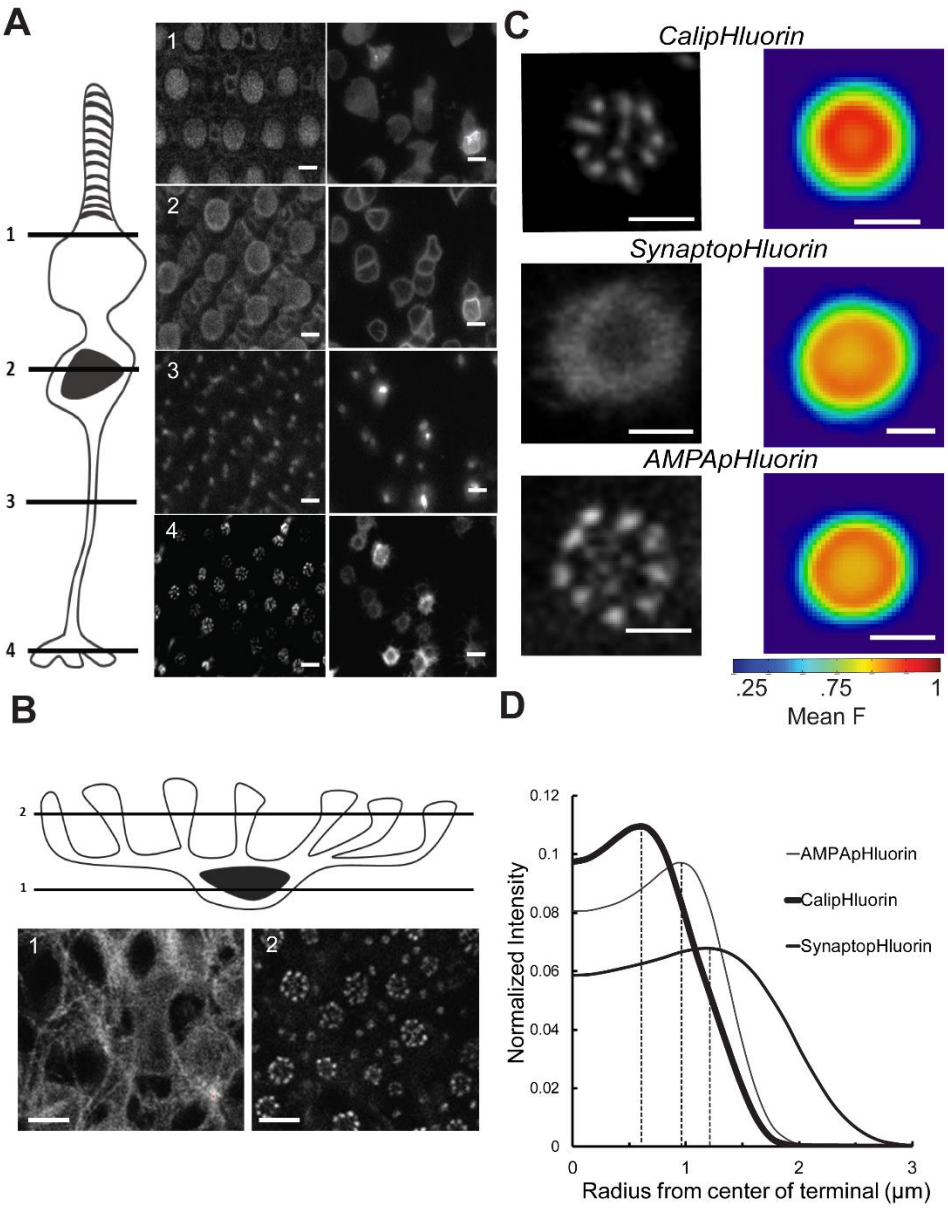

Figure 3. Spatial profiles of CalipHluorin, SynaptopHluorin and AMPApHluorin fluorescence in darkness.

(A) Diagram of a cone with optical planes of section (numbered 1-4). CalipHluorin (central panel) and SynaptopHluorin fluorescence (right panel) at the 2 imaging planes. Scale bar=5 µM. (B) Diagram of a HC with optical planes of section for imaging. (numbered 1-2). AMPApHluorin fluorescence is detected throughout HCs, but especially intense in rosettes at cone terminals and individual puncta at rod terminals. Scale bar=5 µM. (C) Representative image (left) and heat maps of fluorescence intensity, averaged over hundreds of terminals (right) from CalipHluorin, SynaptopHluorin, and AMPApHluorin expressing retinas. Scale bar=2 µM. (D) Distribution of fluorescence as a function of distance from the center of each probe.

SynaptopHluorin reports synaptic cleft pH changes resulting from HC feedback

Once we established the fluorescence of the pHluorin probes in darkness, we investigated how light stimuli lead to a change in fluorescence. Our previous studies showed that light stimuli lead to a 5% increase in CalipHluorin fluorescence, indicating alkalinization of ~0.2 pH units in the synaptic cleft (Wang et al., 2014). Since we could not image during the light flash, we had to measure the remaining "tail" of the fluorescence change immediately after the 508 ms light flash. Therefore the brief acidification of extracellular pH caused by cone synaptic vesicle exocytosis [~10 msec; (DeVries, 2001)] was undetectable, as reported previously for CalipHluorin (Wang et al., 2014). We asked whether synaptopHluorin, also on cone terminals, similarly registers HC-dependent alkalinization with light stimuli (Figure 4). To stimulate a cone light response and trigger consequent HC feedback, we applied a single 500 msec flash of full-field light while imaging with repeated 2-photon scans at 125 msec intervals. By comparing synaptopHluorin fluorescence immediately after the flash (F) to that measured before the flash (F_0), we observed that the stimulus caused a 2% increase in fluorescence (F/F_0=1.019 ± 0.005; n=15 , p =1 x 10^{-6}) (Figure 4A, D), smaller (p =2.2 x 10^{-5}) than the previously measured change in CalipHluorin [~5%; (Wang et al., 2014)], but still indicating significant alkalinization. SynatopHluorin has been used extensively as a probe for exocytosis (Sankaranarayanan and Ryan, 2000), but light decreases cone exocytosis (Rea et al., 2004). Thus, the fluorescence increase triggered by the light flash in these experiments is inconsistent with an exocytotic-induced decrease in the density of probes on the cell surface. Instead, we propose that the fluorescence increase is caused by alkalinization of the synaptic cleft, as we showed previously with CalipHluorin (Wang et al., 2014).

Fluorescence was brightest immediately after the flash and returned to baseline within 500 ms, similar to the time course of the change in CalipHluorin fluorescence after a flash (Wang et al., 2014). Like CalipHluorin, the change in synaptopHluorin fluorescence was eliminated by substituting the weak pH buffer bicarbonate (25 mM) with the stronger and faster pH buffer HEPES (20 mM) (F/F_0=1.003±0.006; n=6 *P*=0.93) (Figure 4B). Also like CalipHluorin, the change in synaptopHluorin fluorescence was eliminated with the AMPA receptor antagonist GYKI (50µM) (F/F_0=1.003± 0.003, n=23 *P*=0.31) (Figure 4A, D), suggesting that the source of the alkalinization was not cones, which have no native AMPA receptors (Haverkamp et al., 2001), but rather HCs, which have native AMPA receptors.

To further determine the source of the alkalinization detected by synaptopHluorin, we stimulated the retina with spots of light while imaging fluorescence in cones located within the center of the spot. If a signal from HCs generates the alkalinization, then a small spot should generate a weaker response than a large spot, as the HC response is caused by a convergence

of inputs from many photoreceptors onto the wide dendritic projections of a HC. An annulus of light (300 µm inner diameter and 1000 µm outer diameter) elicited a similar change in fluorescence as a full field light stimulus (F/F_0=1.017 ± 0.003, n=15 *p* = 0.0002), and was blocked by GYKI (1.005± 0.003, n=8 p =0.086) (Figure 4C, D), indicating that alkalinization can be detected even though cones in the 50 µm central area were not directly exposed to light. Consistent with summation over a large collecting area, we found that a small spot (50 µM diameter) that covers only the imaged area (50 µM diameter) elicited no significant synaptopHluorin response (F/F_0=1.006 ± 0.003, n=15, p = 0.058) (Figure 4A, D), whereas larger spots elicited significant responses that grew increasingly strong up to a diameter of 500 µm (p <0.001) (Figure 4D), typical of the dendritic tree diameter of HCs in zebrafish retina (Daniels and Baldridge, 2011). Hence the receptive field characteristics of the synaptopHluorin response are consistent with signaling by laterally projecting HCs.

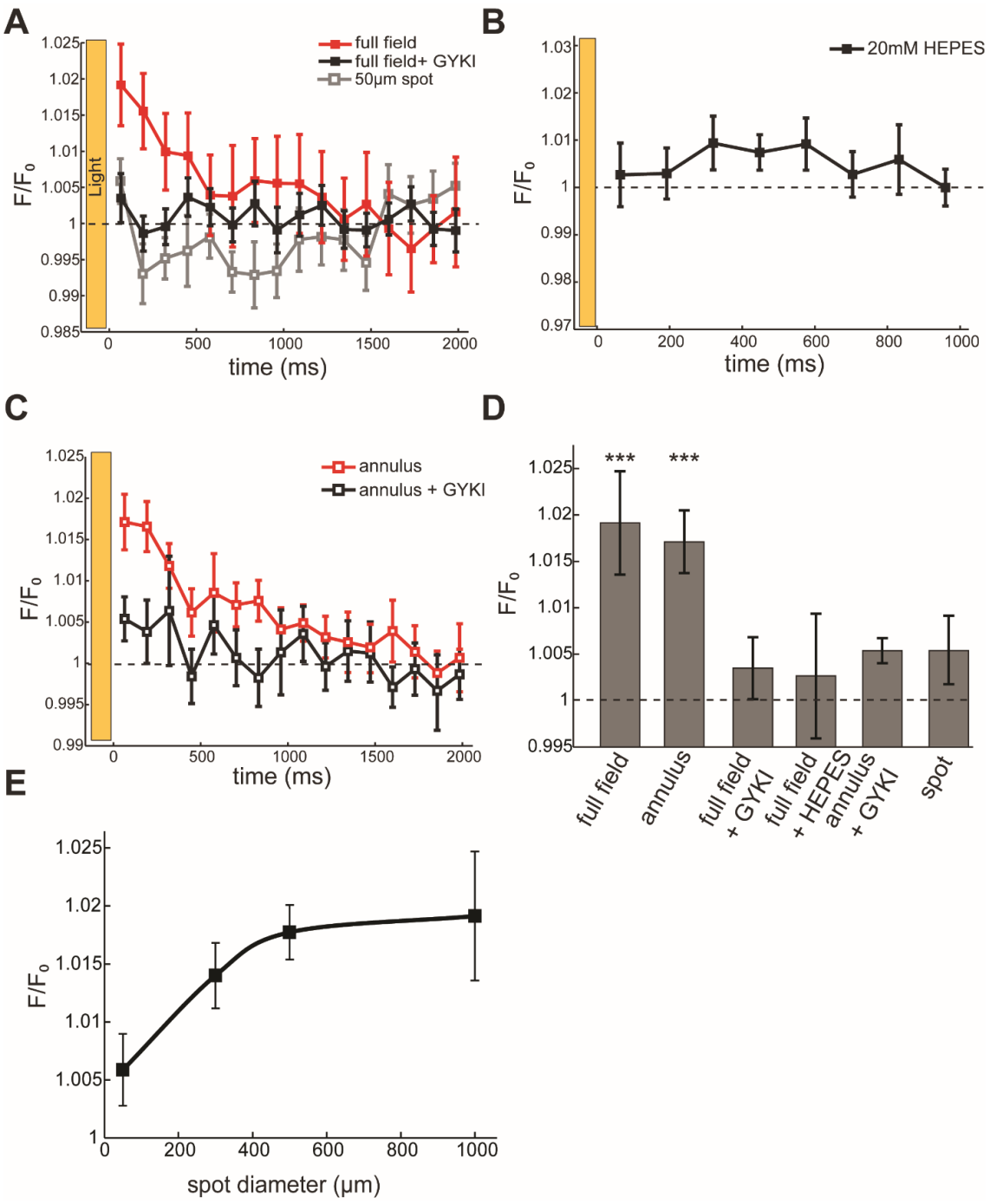

Figure 4: SynaptopHluorin reports HC-mediated changes in pH after a light flash.
Images of SynaptopHluorin expression cone terminals were collected before a light flash and for ~2 sec after the light flash. (A) Fluorescence intensity was brightest immediately after the light flash (yellow bar). Full-field illumination for 0.5 s caused a 1.9% increase in average pixel intensity at the terminals. This response was not present when using a 50 µm spot stimulus. (A-C) Both HC feedback inhibitors, GYKI and HEPES, abolish the light-elicited pH response. (C) Similarly to CalipHluorin, the pH response can be driven by surround illumination with an annulus (inner diameter, 300 µm; outer diameter, 1,000 µm, excluding the imaged area). (D) Group data of the initial change in SynaptopHluorin fluorescence at the first time point (125 msec) after the light flash and under different experimental conditions. Statistical comparisons are with respect to F/F_0=1.0. (E) SynaptopHluorin

fluorescence increases with spot diameter reaching a maximum at 500µm. Unless otherwise noted, sample sizes for each experimental condition represent independent frames imaged from at least 4 zebrafish retinas with the mean fluorescence of many individual terminals averaged to give a single value for each frame. In this and other figures, variability among data is expressed as mean ±SEM and * denotes p <0.05, ** denotes p <0.01, *** denotes p <0.001.

To verify that HCs are the source of the pH change detected by synaptopHluorin, we bypassed the photoreceptors entirely and directly manipulated the membrane potential of HCs. We employed a depolarizing ligand-gated ion channel and a complementary ligand, both of which originated from invertebrate nervous systems and are foreign to zebrafish. SynaptopHluorin fish were crossed with transgenic fish expressing the alien channel, named FaNaC [FMRFamide (PheMetArgPhe-NH2)-gated Na^+ channel] (Lingueglia et al., 1995). HC- specific expression was driven with the promoter for connexin 55.5. The SynaptopHluorin-FaNaC fish showed a decrease in fluorescence in response to 30µM FMRFamide, consistent with depolarization of HCs, causing acidification of the synaptic cleft (F/F_0=0.828 ± 0.02, n=7, p = 0.0005). SynaptopHluorin fish that did not express FaNaC showed no change in fluorescence (F/F_0=0.999 ± 0.005, n=5, p = 0.99) (Figure 5). The FMRFamide-induced acidification occurred even when cone Ca^{2+} channels were blocked with nifedipine and HC AMPA receptors were blocked with GYKI (F/F_0=0.841 ± 0.04, n=6, p = 0.038 compared to controls, p = 0.90 compared to FMRFamide only) (Figure 5). This result indicates that FMRFamide-elicited change in pH is mediated by HCs, and is not dependent on cones.

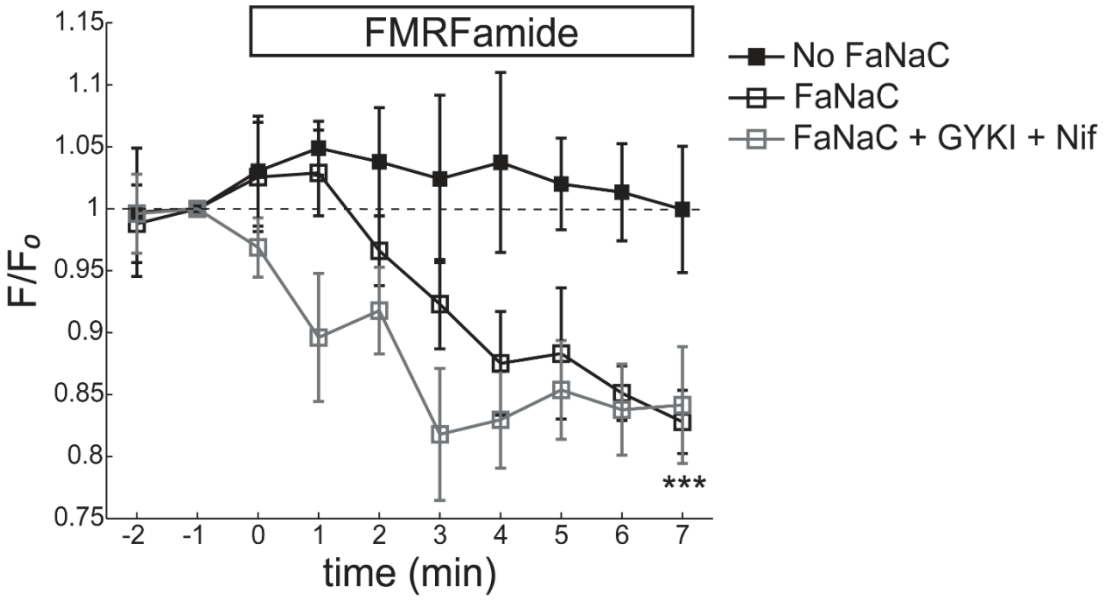

Figure 5. SynaptopHluorin reports changes in pH after agonist-induced depolarization of HCs.
Double transgenic fish carrying SynaptopHluorin in cones and FaNaC in horizontal cells were generated by crossing SynaptopHluorin and FaNaC fish lines. 30µM FMRFamide added at time zero caused a decrease in SynaptopHluorin fluorescence in retinas from the double transgenic fish (*** denotes p = 0.0005) but not in the retina from the SynaptopHluorin single transgenic fish. Pre-incubation with GYKI and Nifedipine did not have an effect on the FMRFamide-elicited acidification, i.e. calcium channels on the HC side are not responsible for this effect.

AMPApHluorin expressed in HC dendrites also reports pH changes in the synaptic cleft.

Next, we turned to AMPApHluorin. Before moving to transgenic expression in zebrafish retina, we verified that AMPApHluorin is sensitive to pH by transfecting CMV-AMPApHluorin into cultured hippocampal neurons from rat and superfusing solutions with different pH values. Fluorescence dropped rapidly (within seconds) in both hippocampal cell somas and dendrites upon acidification of extracellular pH from 7.4 to 6, and was fully restored when pH was raised to 7.4, consistent with pHluorin displayed on the cell surface (Sankaranarayanan and Ryan, 2000). In contrast, no signal was detected in AMPApHluorin-free neurons that had been pre-loaded with 20µM SNARF, an intracellular fluorescent pH indicator. As a further test for cell-surface origin of the fluorescence signal, we modified AMPApHluorin by inserting a thrombin proteolytic cleavage site between the extracellular pHluorin region and the AMPA receptor. Thrombin (10 U/ml) treatment of cells expressing this construct resulted in elimination of cell-surface fluorescence, verifying that AMPApHluorin on the cell surface.

We next asked whether AMPApHluorin, expressed in the transgenic zebrafish retina on HCs, can detect a change in pH mediated by synaptic feedback (Figure 6A). Following a light flash, we observed a small but significant, increase in fluorescence (1%) during the first scan after light offset (F/F_0=1.010 ± 0.005, n=17; p = 0.0025) decaying to baseline in later scans. The initial increase was detected in terminals, but not in HC somata (F/F_0=0.998 ± 0.002 n=23, p = 0.63) (Figure 6A). These results suggest that AMPApHluorin on the HCs does detect synaptic alkalinization. However, because on the probe is located, on the average, further from its source (Figure 3C, D), the signal is smaller than that detected by CalipHluorin ($p = 2.2 \times 10^{-5}$). The 1% difference in fluorescence detected by AMPApHluorin was not statistically different from the 2% change detected by SynaptopHluorin (p = 0.07).

To further verify that the fluorescence change in retina originates from AMPApHluorin on the HC cell surface and not intracellular compartments, we measured the effect of changing extracellular pH, achieved by washing with saline containing MES (20mM), a membrane-impermeant pH buffer. The initial normalized fluorescence (F/F_0=1 ± 0.09, n=20) dropped after changing the extracellular pH from 7.4 to 5.5 (F/F_0=0.1 ± 0.03, n=20, $p = 2.3 \times 10^{-10}$), reversing upon return to pH 7.4 (F/F_0=1.02 ± 0.11, p = 0.8). The accessibility of AMPApHluorin to extracellular pH change is once again consistent with cell-surface origin of the signal.

In addition to responding to light-induced HC feedback, AMPApHluorin also responded to application of an agonist or competitive antagonist of the ionotropic glutamate receptors on HCs. Addition of AMPA (20 µM), led to a decrease in AMPApHluorin fluorescence of 17% (F/F_0=0.837 ± 0.04, n=14, p = 0.0037) (Fig 6B), consistent with depolarization of HCs causing acidification of the extracellular pH. By contrast, an antagonist of the receptors, GYKI (50 µM), led to an increase of in fluorescence of 11% (1.105 ± 0.037, n=8, p = 0.013) (Fig 6B), consistent with hyperpolarization of HCs alkalinizing extracellular pH.

As explained earlier, the magnitude of AMPApHluorin fluorescence depends on two factors: the expression density of the probe on the cell surface, and the value of the extracellular pH. We considered the possibility that HC voltage changes might lead to a change in the cell surface density of AMPApHluorin. AMPA receptors are inserted into the plasma membrane by exocytosis and removed by endocytosis, but activity-dependent alteration of both processes requires many minutes, both in neurons in the brain (Wang and Linden, 2000; Passafaro et al., 2001) and the retina (Xia et al., 2006; Casimiro et al., 2013). In contrast, the light-elicited AMPApHluorin signal occurs within 1 sec (see Figure 6A). Moreover, AMPA receptor endocytosis is dependent on clathrin and dynamin and it is blocked by the dynamin inhibitor dynasore (Macia et al., 2006). We found that the agonist-induced decrease in AMPApHluorin signal is unaffected by 80 µM dynasore (0.83 ± 0.11, n=10, p = 0.02) (Figure 6C, D). Taken together, these results suggest that changes in the AMPApHluorin signal reflects a change in the extracellular pH, and not a change in the number of probes on the surface of a cell.

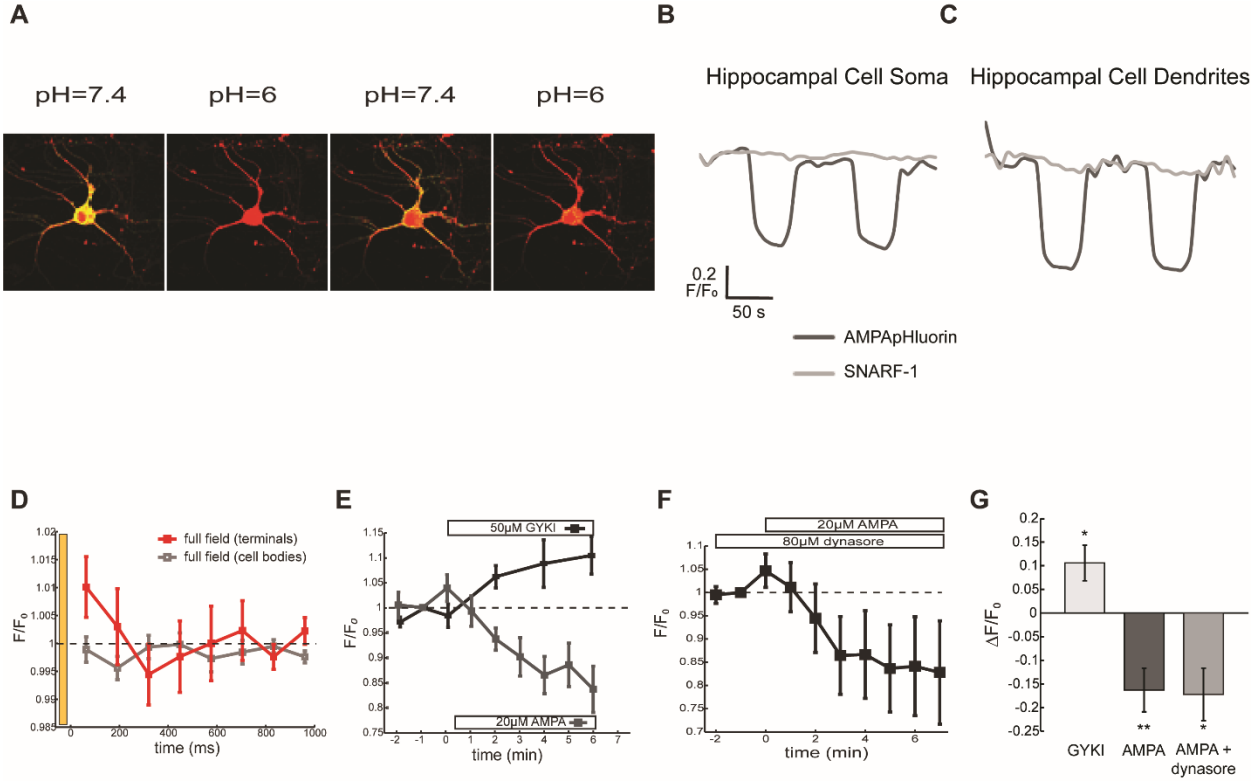

Figure 6. AMPApHluorin expressed in HC dendrites reports changes in pH in the synaptic cleft. (A) During the first scan after a light flash (yellow bar), AMPApHluorin fluorescence (F) was increased by 1% as compared to the pre-flash level (F_0). No fluorescence change was reported by AMPApHluorin in HC somata. (B) AMPApHluorin fluorescence in isolated retinae was monitored after treatment with either GYKI or AMPA. GYKI induced an increase in AMPApHluorin fluorescence indicating trafficking of GluR2 to the HC terminal surface. In contrast, AMPA treatment led to an internalization of GluR2 as demonstrated by the decrease of AMPApHluorin fluorescence on the HC terminal surface. Together, this shows that AMPApHluorin can serve as a receptor for GluR2 trafficking and that HCs exhibit some form of plasticity. * denotes p <0.05 ** denotes p <0.01 (C) Application of dynasore (80 µM) had no effect on the decrease in fluorescence noted after the application of AMPA. (D) Bar graph presentation of the results in figures B-C. (E) Fluorescence images of a dissociated cultured hippocampal

neuron, transfected with CMV-AMPApHluorin superfused with buffer solutions at varying pH. (F) The fluorescence intensity of cell soma (G) and dendrites dropped upon applying acidic the extracellular buffer solution from pH 7.4 to 6 and recovered after returning to pH 7.4. (H) AMPApHluorin fluorescence was reversible and quenched to the background level after superfusing the retina with pH 5.5 solution. Accessibility to buffer is consistent with the signal arising from probes on the cell-surface. Data is plotted as Mean ± SEM.

pH changes are locally constrained

Synaptically released glutamate can spill-over not only between individual ribbon-associated active zones within a cone terminal, but between different cone terminals, resulting in cross-talk (Szmajda and Devries, 2011). This raises the question of whether protons spill over between invaginations within an individual terminal and whether they spill over between different terminals. We measured the minimal path length a proton would need to travel to get from the base of one ribbon, where HC feedback appears to be focused, to a neighboring ribbon. We analyzed electron micrograph sections that included at least 2 ribbons, each terminating at the presynaptic membrane (Figure 7A). The average minimal extra-cellular distance measured between ribbon bases was 4,908 ± 655 nm; range 567-13,316 nm n=56, Figure 7B).

How does the profile of pH measured by the three pHluorin probes compare with the inter-ribbon distance? The voltage-gated Ca^{2+} channels that control neurotransmitter release are situated 200-300 nm from ribbons (Raviola and Gilula, 1975). Consequently, the CalipHluorin, which is derived from a subunit of the channel, is also located at this site, as confirmed by our immunolabeling results (Fig. 2). After a flash of light, the fluorescence change reported by CalipHluorin (Wang et al., 2014), SynaptopHluorin (Fig. 4a) and AMPApHluorin (Fig. 6a) are 5%, 2%, and 1%, respectively (Fig. 7C), correlated with their average distance from the ribbon (see Figure 3D).

Taking this into account, an exponential fit of the pH profile predicts no significant signal at the average inter-ribbon distance of ~4.9 µm, almost 90% decline of the signal at the minimum measured inter-ribbon distance of ~1 µm, exhibited by <5% of observed ribbon pairs. Even more attenuated is signal spread to neighboring cone terminals. The specific profile of the pH signal depends on the uniformity of the extracellular pH buffers and the proton transporters along the cleft, but our results make significant proton spillover very unlikely.

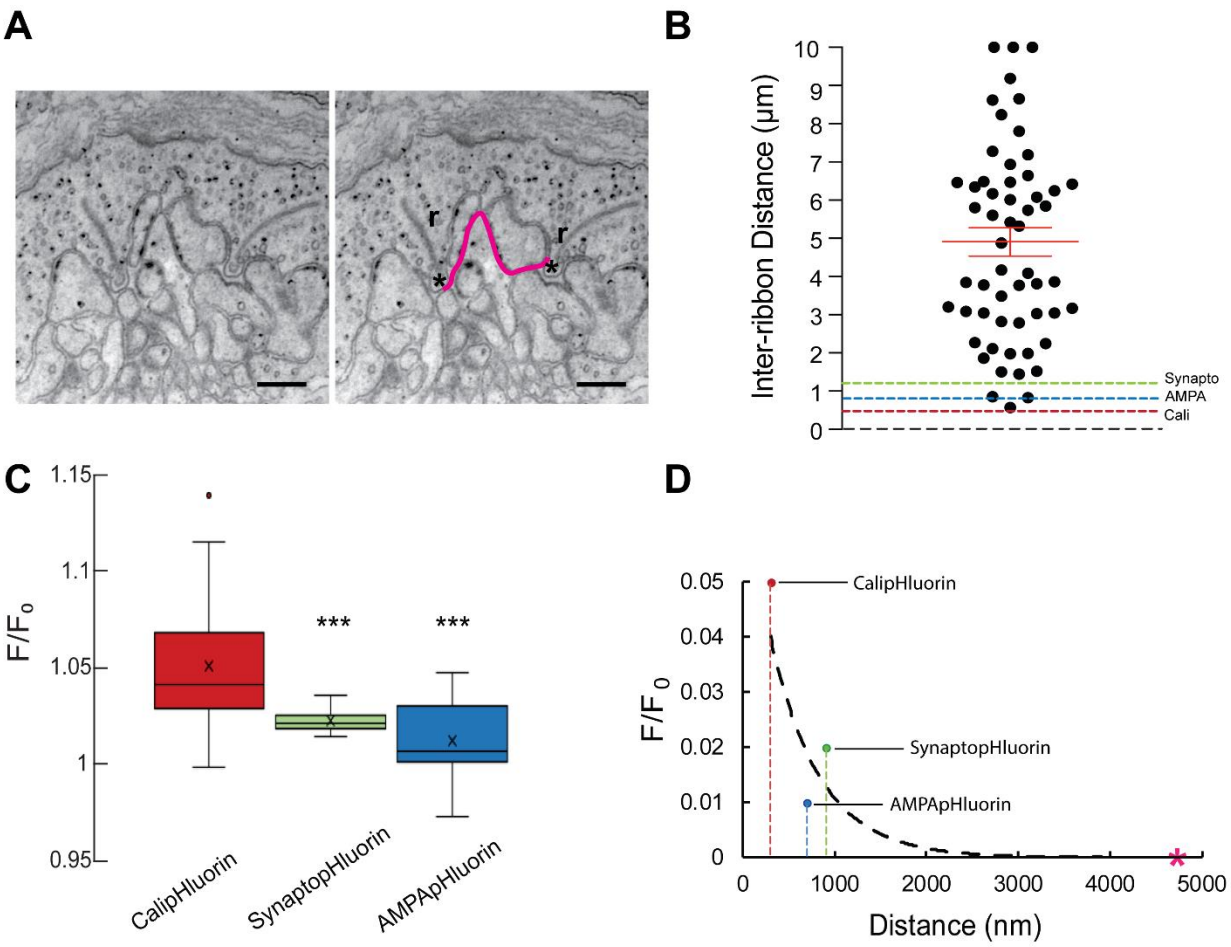

Figure 7. pH changes drop rapidly with distance and are likely constrained to each invagination.

(A) Electron micrographs from synaptic invaginations of zebrafish. The shortest extracellular path was measured between the bases of adjacent ribbons, where they abut the plasma membrane (n=56). Ribbons are marked with r, arcuate density at the ribbon base is marked with *. Scale bar =500nm. (B) Distribution of inter-ribbon distances, with a mean value of 4,908 ± 655 nm. (C) Summary of the average change in fluorescence after a light flash reported by each of the 3 pH probes. CalipHluorin results were adapted from Wang et al. 2014. Analysis was performed with one way ANOVA, F (2. 53) = 13.21, p =2.2 x 10^{-5}. (D) The change in fluorescence with distance from the ribbon was fitted to the exponential curve using the equation $y=0.0702e^{-0.002x}$ (R^2=0.4989) based on the locations of peak radial intensity for each probe (see Figure 3D), with CalipHluorin at 300 nm from the ribbon. The predicted change in fluorescence at the average inter-ribbon distance is marked with an asterisk.

DISCUSSION

pHluorin as a tool for mapping pH gradients

A variety of tools have been used to measure extracellular pH and elucidate the role of protons as a putative neurotransmitter in the nervous system. For many decades, pH-specific microelectrodes have been available for measuring pH in the extracellular space (Chesler, 1990). However, these electrodes were invasive and difficult to manufacture, and suffered from

high noise, greatly limiting spatial and temporal resolution. To lower noise, a self-referencing pH electrode was devised by repeatedly vibrating the probe between two extracellular positions (Kreitzer et al., 2007). While this system is accurate and fast, it cannot be used in the intact retina without disrupting the complex architecture of synaptic connections.

Fluorescent biosensors for pH, such as seminaphtharhodafluor (SNARF), can be used for non-invasive optical detection of pH changes (Buckler and Vaughan-Jones, 1990). However, rapid diffusion of this small molecule precludes spatial resolution of pH gradient at the scale of a cone terminal. Finally, genetically-encoded pH sensors based on pHluorin can be expressed in a cell-type specific fashion to sense pH changes at an individual synapse (Miesenbock et al., 1998). pHluorin can be spliced onto a wide variety of protein platforms, to detect the fusion of synaptic vesicles with the plasma membrane, or to follow protein trafficking to or from cell surface (Rajappa et al., 2016). Here we are using pHluorin to report on rapid changes in pH, entirely in the extracellular space. By attaching pHluorin to protein platforms that are displayed on the cell surface but differ in their precise location, we have mapped the pH profile in the synaptic cleft and identified the region very near the synaptic ribbon as the crucial spot with the largest HC feedback-elicited pH change.

The proton hypothesis of negative feedback in the outer retina.

According to the pH hypothesis of negative feedback, the hyperpolarization of the HC membrane potential during the light response drives influx of protons through a channel or transporter in HC dendrites, leading to alkalinization of the synaptic cleft reviewed in (Kramer and Davenport, 2015). Alternative scenarios have also been proposed that could more indirectly change extracellular pH in response to a voltage change in HCs. These include transport of the pH buffer bicarbonate across the HC membrane (Warren et al., 2016b), or flux of ATP through pannexin channels, which through ecto-ATPase-elicited hydrolysis, may lead to liberation of protons in the synaptic cleft (Vroman et al., 2014). While there is debate about the relatively importance of these mechanisms for changing extracellular proton concentration, there is a growing consensus that the change in extracellular pH is the crucial event that alters the gating of L-type Ca^{2+} channels in cones, changing the rate of Ca^{2+}-dependent exocytosis of glutamate-filled synaptic vesicles at the synaptic ribbon (Thoreson and Mangel, 2012; Kramer and Davenport, 2015). It should be noted that fusion of these vesicles also contributes protons to the extracellular space, which itself inhibits L-type Ca^{+2} channels (DeVries, 2001); however, this process is too transient to be detected by CalipHluorin (Wang et al., 2014).

Various lines of evidence support the hypothesis that a pH change is the critical signal responsible for negative feedback. Artificially acidifying or alkalinizing the synaptic cleft modulates the voltage-dependent gating of cone Ca^{2+} channels, enough to account for HC feedback (Davenport et al., 2008; Fahrenfort et al., 2009). Adding a strong pH buffer, such as HEPES, suppresses HC feedback (Trenholm and Baldridge, 2010; Hirasawa and Kaneko, 2003)

and eliminates the antagonistic receptive field surround of neurons further along in the visual system (Davenport et al., 2008). Finally, the development of CalipHluorin as a genetically-encoded pH probe has enabled direct demonstration of synaptic cleft akalinization in response to HC hyperpolarization (Wang et al., 2014). Our current results with SynaptopHluorin and AMPApHluorin add new evidence further supporting the pH hypothesis.

Spatial spread and constraint of synaptic signals in the outer retina.

The ribbon synapse lies in the deepest recess of an invagination formed within the cone terminal. Muller glial cells wrap around the terminal and possess glutamate transporters that actively remove glutamate from the extracellular space (Burris et al., 2002; Sarthy et al., 2005). Despite these impediments, results from paired cone-cone patch clamp recordings show that glutamate can spill over, operating in milliseconds to spread light-elicited signals between neighboring terminals in the cone network (Szmajda and Devries, 2011). In contrast, our results suggest that the HC feedback-induced pH change at one cone terminal does not substantially spill over to neighboring cones. Even though our 3 probes all contain the identical pH sensor (i.e. pHluorin), they are displayed in different locations in the synaptic cleft and consequently, they exhibited different magnitude changes in fluorescence after a full-field light stimulus. CalipHluorin, tightly localized near the ribbon, registered a 5% increase in fluorescence after light [Figure 2C, (Wang et al., 2014)]. SynaptopHluorin, more broadly displayed throughout cone terminals, registered a 2% increase in fluorescence (Figure 4A). AMPApHluorin, on the HC dendrites and somata, registered a 1% increase (Figure 6A). All 3 probes were over-expressed in the zebrafish retina, so probe locations do not exactly reflect the normal distribution of the parent protein in WT fish. Nonetheless, probe locations seen with 2-photon imaging are consistent with the patterns of the native parent proteins described previously (Morgans et al., 1996; Morgans, 2001; Klooster et al., 2009; De Sevilla Muller et al., 2013). These include rosettes of Caliphluorin and AMPAphluorin that correspond to ultrastructural observation of clusters of Ca2+ channel proteins (Lv et al., 2012) and AMPA receptor subunits (Klooster et al., 2009), respectively. By appearing at different geographic locations, the probes allow quantitative comparison of the pH change at different positions relative to the synaptic ribbon, a common geographic landmark.

Hence the feedback mechanism that controls synaptic pH appears to be focused at the site where it can have the largest effect on cone neurotransmitter release. Moreover, the sharp decline in the HC feedback-elicited change in fluorescence with probes located further from the ribbon suggests little or no spill-over of pH transients from illuminated cones to non-illuminated neighbors, at least following brief (msec to seconds) light flashes. It is possible that pH fluctuates in a more coordinated manner during longer-term light or dark adaptation (Dmitriev and Mangel, 2004), but our results suggest that there is little cross-talk between cone terminals during dynamic changes in visual scenes.

The lack of cross-talk is consistent with strong pH buffers and transporters removing protons from the extracellular space, as well as the tortuous and narrow path that protons must travel to affect neighboring terminals. Glutamate spillover requires only that the neurotransmitter reach glutamate receptors or transporters, which are widely distributed all over a neighboring terminal (Haverkamp et al., 2000). In contrast, pH spillover would require diffusion of protons all the way out of one invagination and all the way up to the apex of another invagination where the L-type Ca^{2+} channels are tightly localized.

Synaptic contacts in cone terminals in zebrafish appear as rosettes (Song et al., 2008), which manifest as a ring of labeled CalipHluorin and AMPApHluorin puncta in our studies. It is interesting that these puncta are evenly spaced and lie near the perimeter of the terminal, suggesting maximization of the distance between nearest neighbors. Cone invaginating synapses typically possess a single bipolar cell dendrite flanked by two lateral HC dendrites. Compartmentalizing pH signals ensures that each invaginating synapse computes feedback independently from neighboring invaginating synapses, complementing independent operation of ribbon-mediated synaptic vesicle release (Grassmeyer and Thoreson, 2017). By maintaining independence of feedback signaling, each invagination could make a unique calculation, collecting and comparing inputs from the two HCs, each with a unique receptive field, and outputting this information to different types of bipolar cells. At the same time, spillover of glutamate between invaginations, and further between terminals, can maximize sensitivity of feedforward signaling.

In addition to negative feedback on cones triggered by HC membrane hyperpolarization, HCs also exert positive feedback, triggered by a change in intracellular Ca^{2+} in HCs (Jackman et al., 2011). Activation of Ca^{2+}-permeant AMPA receptors in HC dendrites triggers Ca^{2+}-dependent release of an unidentified neurotransmitter that enhances cone neurotransmitter release. Interestingly, the spatial spread of the intracellular triggers for negative and positive feedback from HCs differ. Negative feedback by HCs is distributed over a large area because membrane hyperpolarization spreads electrotonically though the low cytoplasmic resistance of an individual HC, and through gap junctions that couple many HCs. In contrast, positive feedback from HCs is spatially limited to individual cone terminals because the spread of intracellular Ca^{2+} is constrained to an individual HC dendrite by cytoplasmic Ca^{2+} buffers. The interplay between spatial spread vs. spatial constraint of both intracellular and extracellular signals is a recurring theme in the outer retina, functioning to adjust both visual sensitivity and visual acuity over a wide range of illumination conditions.

ACKNOWLEDGEMENTS

We thank S. Brockerhoff (University of Washington), M. Kamermans (Netherlands Institute for Neuroscience), R. Huganir (Johns Hopkins University School of Medicine) and A.R. McQuiston (Virginia Commonwealth University School of Medicine) for providing plasmids. We thank Joe

DeGiorgis for assisting with EM microscopy, Benjamin E Smith for assisting with image analysis for figure 3D and Chris Habrian for assisting with pH Calibration for figure 1C. This work was supported by grants from the US National Institutes of Health to R.H.K. (R01 EY024334 and P30 EY003176) and to T.M.W (F32 EY020095).

AUTHOR CONTRIBUTION

Conceptualization, B.B.C, L.C.H., T.M.W and R.H.K.; Methodology, B.B.C, L.C.H., T.M.W, R.R and R.H.K.; Formal Analysis B.B.C, L.C.H, T.M.W, and R.R; Investigation, B.B.C, L.C.H, T.M.W and R.R; Writing – Original Draft, R.H.K and B.B.C; Writing – Review & Editing, R.H.K, B.B.C and R.R, Visualization, B.B.C; Funding Acquisition, T.M.W and R.H.K; Resources, R.H.K, L.C.H, T.M.W and B.B.C; Supervision, R.H.K.

DECLARATION OF INTERESTS

The authors declare no competing interests

CITATIONS

Ashby MC, De La Rue SA, Ralph GS, Uney J, Collingridge GL, Henley JM (2004) Removal of AMPA receptors (AMPARs) from synapses is preceded by transient endocytosis of extrasynaptic AMPARs. J Neurosci 24:5172-5176.

Buckler KJ, Vaughan-Jones RD (1990) Application of a new pH-sensitive fluoroprobe (carboxy-SNARF-1) for intracellular pH measurement in small, isolated cells. Pflugers Arch 417:234-239.

Burris C, Klug K, Ngo IT, Sterling P, Schein S (2002) How Muller glial cells in macaque fovea coat and isolate the synaptic terminals of cone photoreceptors. J Comp Neurol 453:100-111.

Byzov AL, Shura-Bura TM (1986) Electrical feedback mechanism in the processing of signals in the outer plexiform layer of the retina. Vision Res 26:33-44.

Cadetti L, Thoreson WB (2006) Feedback effects of horizontal cell membrane potential on cone calcium currents studied with simultaneous recordings. J Neurophysiol 95:1992-1995.

Campbell FW, Robson JG (1968) Application of Fourier analysis to the visibility of gratings. J Physiol 197:551-566.

Casimiro TM, Nawy S, Carroll RC (2013) Molecular mechanisms underlying activity-dependent AMPA receptor cycling in retinal ganglion cells. Mol Cell Neurosci 56:384-392.

Cendese V, de Graff W, Csikos T, Poovayya M, Zoidl G, Kamermans M (2017) Pannexin 1 is critically involved in feedback from horizontal cells to cones. Front Mol Neurosci 10(403):1-13.

Chapot CA, Behrens C, Rogerson LE, Baden T, Pop S, Berens P, Euler T, Schubert T (2017) Local signals in mouse horizontal cell dendrites. Curr Bio 27(23):3603-3615.e5.

Chesler M (1990) The regulation and modulation of pH in the nervous system. Prog Neurobiol 34:401-427.

Daniels BA, Baldridge WH (2011) The light-induced reduction of horizontal cell receptive field size in the goldfish retina involves nitric oxide. Vis Neurosci 28:137-144.

Davenport CM, Detwiler PB, Dacey DM (2008) Effects of pH buffering on horizontal and ganglion cell light responses in primate retina: evidence for the proton hypothesis of surround formation. J Neurosci 28:456-464.

De Sevilla Muller LP, Liu J, Solomon A, Rodriguez A, Brecha NC (2013) Expression of voltage-gated calcium channel alpha(2)delta(4) subunits in the mouse and rat retina. J Comp Neurol 521:2486-2501.

Denk W, Detwiler PB (1999) Optical recording of light-evoked calcium signals in the functionally intact retina. Proc Natl Acad Sci U S A 96:7035-7040.

DeVries SH (2001) Exocytosed protons feedback to suppress the Ca2+ current in mammalian cone photoreceptors. Neuron 32:1107-1117.

Dmitriev AV, Mangel SC (2004) Retinal pH reflects retinal energy metabolism in theday and night. J Neurophysiol 91(6):2404-12.

Fahrenfort I, Steijaert M, Sjoerdsma T, Vickers E, Ripps H, van Asselt J, Endeman D, Klooster J, Numan R, ten Eikelder H, von Gersdorff H, Kamermans M (2009) Hemichannel-mediated and pH-based feedback from horizontal cells to cones in the vertebrate retina. PLoS One 4:e6090.

Grassmeyer JJ, Thoreson WB (2017) Synaptic Ribbon Active Zones in Cone Photoreceptors Operate Independently from One Another. Front Cell Neurosci 11:198.

Haverkamp S, Grunert U, Wassle H (2000) The cone pedicle, a complex synapse in the retina. Neuron 27:85-95.

Haverkamp S, Grunert U, Wassle H (2001) The synaptic architecture of AMPA receptors at the cone pedicle of the primate retina. J Neurosci 21:2488-2500.

Hirasawa H, Kaneko A (2003) pH changes in the invaginating synaptic cleft mediate feedback from horizontal cells to cone photoreceptors by modulating Ca2+ channels. J Gen Physiol 122:657-671.

Holzhausen LC, Lewis AA, Cheong KK, Brockerhoff SE (2009) Differential role for synaptojanin 1 in rod and cone photoreceptors. J Comp Neurol 517:633-644.

Jackman SL, Babai N, Chambers JJ, Thoreson WB, Kramer RH (2011) A positive feedback synapse from retinal horizontal cells to cone photoreceptors. PLoS Biol 9:e1001057.

Kamermans M, Fahrenfort I, Schultz K, Janssen-Bienhold U, Sjoerdsma T, Weiler R (2001) Hemichannel-mediated inhibition in the outer retina. Science 292:1178-1180.

Kennedy BN, Alvarez Y, Brockerhoff SE, Stearns GW, Sapetto-Rebow B, Taylor MR, Hurley JB (2007) Identification of a zebrafish cone photoreceptor-specific promoter and genetic rescue of achromatopsia in the nof mutant. Invest Ophthalmol Vis Sci 48:522-529.

Klooster J, Yazulla S, Kamermans M (2009) Ultrastructural analysis of the glutamatergic system in the outer plexiform layer of zebrafish retina. J Chem Neuroanat 37:254-265.

Kramer RH, Davenport CM (2015) Lateral Inhibition in the Vertebrate Retina: The Case of the Missing Neurotransmitter. PLoS Biol 13:e1002322.

Kreitzer MA, Collis LP, Molina AJ, Smith PJ, Malchow RP (2007) Modulation of extracellular proton fluxes from retinal horizontal cells of the catfish by depolarization and glutamate. J Gen Physiol 130:169-182.

Kwan KM, Fujimoto E, Grabher C, Mangum BD, Hardy ME, Campbell DS, Parant JM, Yost HJ, Kanki JP, Chien CB (2007) The Tol2kit: a multisite gateway-based construction kit for Tol2 transposon transgenesis constructs. Dev Dyn 236:3088-3099.

Lingueglia E, Champigny G, Lazdunski M, Barbry P (1995) Cloning of the amiloride-sensitive FMRFamide peptide-gated sodium channel. Nature 378:730-733.

Lv P, Sihn CR, Wang W, Shen H, Kim HJ, Rocha-Sanchez SM, Yamoah EN (2012) Posthearing Ca(2+) currents and their roles in shaping the different modes of firing of spiral ganglion neurons. J Neurosci. 14;32(46):16314-30.

Macia E, Ehrlich M, Massol R, Boucrot E, Brunner C, Kirchhausen T (2006) Dynasore, a cell-permeable inhibitor of dynamin. Dev Cell 10:839-850.

Mercer AJ, Chen M, Thoreson WB (2011) Lateral mobility of presynaptic L-type calcium channels at photoreceptor ribbon synapses. J Neurosci 31:4397-4406.

Miesenbock G, De Angelis DA, Rothman JE (1998) Visualizing secretion and synaptic transmission with pH-sensitive green fluorescent proteins. Nature 394:192-195.

Morgans CW (2001) Localization of the alpha(1F) calcium channel subunit in the rat retina. Invest Ophthalmol Vis Sci 42:2414-2418.

Morgans CW, Brandstatter JH, Kellerman J, Betz H, Wassle H (1996) A SNARE complex containing syntaxin 3 is present in ribbon synapses of the retina. J Neurosci 16:6713-6721.

Passafaro M, Piech V, Sheng M (2001) Subunit-specific temporal and spatial patterns of AMPA receptor exocytosis in hippocampal neurons. Nat Neurosci 4:917-926.

Pologruto TA, Sabatini BL, Svoboda K (2003) ScanImage: flexible software for operating laser scanning microscopes. Biomed Eng Online 2:13.

Provost E, Rhee J, Leach SD (2007) Viral 2A peptides allow expression of multiple proteins from a single ORF in transgenic zebrafish embryos. Genesis 45:625-629.

Rajappa R, Gauthier-Kemper A, Boning D, Huve J, Klingauf J (2016) Synaptophysin 1 Clears Synaptobrevin 2 from the Presynaptic Active Zone to Prevent Short-Term Depression. Cell Rep 14:1369-1381.

Raviola E, Gilula NB (1975) Intramembrane organization of specialized contacts in the outer plexiform layer of the retina. A freeze-fracture study in monkeys and rabbits. J Cell Biol 65:192-222.

Rea R, Li J, Dharia A, Levitan ES, Sterling P, Kramer RH (2004) Streamlined synaptic vesicle cycle in cone photoreceptor terminals. Neuron 41:755-766.

Sankaranarayanan S, Ryan TA (2000) Real-time measurements of vesicle-SNARE recycling in synapses of the central nervous system. Nat Cell Biol 2:197-204.

Sarthy VP, Pignataro L, Pannicke T, Weick M, Reichenbach A, Harada T, Tanaka K, Marc R (2005) Glutamate transport by retinal Muller cells in glutamate/aspartate transporter-knockout mice. Glia 49:184-196.

Schanuel SM, Bell KA, Henderson SC, McQuiston AR (2008) Heterologous expression of the invertebrate FMRFamide-gated sodium channel as a mechanism to selectively activate mammalian neurons. Neuroscience 155:374-386.

Schmitz F, Konigstorfer A, Sudhof TC (2000) RIBEYE, a component of synaptic ribbons: a protein's journey through evolution provides insight into synaptic ribbon function. Neuron 28:857-872.

Schwartz EA (1982) Calcium-independent release of GABA from isolated horizontal cells of the toad retina. J Physiol 323:211-227.

Shields CR, Klooster J, Claassen Y, Ul-Hussain M, Zoidl G, Dermietzel R, Kamermans M (2007) Retinal horizontal cell-specific promoter activity and protein expression of zebrafish connexin 52.6 and connexin 55.5. J Comp Neurol 501:765-779.

Song PI, Matsui JI, Dowling JE (2008) Morphological types and connectivity of horizontal cells found in the adult zebrafish (Danio rerio) retina. J Comp Neurol 506:328-338.

Svoboda K, Yasuda R (2006) Principles of two-photon excitation microscopy and its applications to neuroscience. Neuron 50:823-839.

Szmajda BA, Devries SH (2011) Glutamate spillover between mammalian cone photoreceptors. J Neurosci 31:13431-13441.

Thoreson WB, Burkhardt DA (1990) Effects of synaptic blocking agents on the depolarizing responses of turtle cones evoked by surround illumination. Vis Neurosci 5:571-583.

Thoreson WB, Mangel SC (2012) Lateral interactions in the outer retina. Prog Retin Eye Res 31:407-441.

Tomita T (1965) Electrophysiological study of the mechanisms subserving color coding in the fish retina. Cold Spring Harb Symp Quant Biol 30:559-566.

Trenholm S, Baldridge WH (2010) The effect of aminosulfonate buffers on the light responses and intracellular pH of goldfish retinal horizontal cells. J Neurochem 115:102-111.

Verweij J, Kamermans M, Spekreijse H (1996) Horizontal cells feed back to cones by shifting the cone calcium-current activation range. Vision Res 36:3943-3953.

Vessey JP, Stratis AK, Daniels BA, Da Silva N, Jonz MG, Lalonde MR, Baldridge WH, Barnes S (2005) Proton-mediated feedback inhibition of presynaptic calcium channels at the cone photoreceptor synapse. J Neurosci 25:4108-4117.

Vroman R, Klaassen LJ, Howlett MH, Cenedese V, Klooster J, Sjoerdsma T, Kamermans M (2014) Extracellular ATP hydrolysis inhibits synaptic transmission by increasing ph buffering in the synaptic cleft. PLoS Biol 12:e1001864.

Wang TM, Holzhausen LC, Kramer RH (2014) Imaging an optogenetic pH sensor reveals that protons mediate lateral inhibition in the retina. Nat Neurosci 17:262-268.

Wang YT, Linden DJ (2000) Expression of cerebellar long-term depression requires postsynaptic clathrin-mediated endocytosis. Neuron 25:635-647.

Warren TJ, Van Hook MJ, Tranchina D, Thoreson WB (2016a) Kinetics of Inhibitory Feedback from Horizontal Cells to Photoreceptors: Implications for an Ephaptic Mechanism. J Neurosci 36:10075-10088.

Warren TJ, Van Hook MJ, Supuran CT, Thoreson WB (2016b) Sources of protons and a role for bicarbonate in inhibitory feedback from horizontal cells to cones in Ambystoma tigrinum retina. J Physiol 594:6661-6677.

Wu SM (1991) Input-output relations of the feedback synapse between horizontal cells and cones in the tiger salamander retina. J Neurophysiol 65:1197-1206.

Xia Y, Carroll RC, Nawy S (2006) State-dependent AMPA receptor trafficking in the mammalian retina. J Neurosci 26:5028-5036.

Chapter 5: Concluding section

In Chapter 4 we were able to successfully express 3 different pH probes in the HC-cone photoreceptor synapse. We exhibited that while all probes are able to detect light induced alkalinization in the invaginated synaptic cleft following a light stimulus, the change in pH was most pronounced when using the CalipHluorin probe, localized to the voltage gated Ca^{2+} channel on cone photoreceptors. Depolarization of HCs when using FMRFamide on fish expressing FaNaC caused a pronounced acidification of the synaptic cleft as measured by synaptopHluorin. These results were consistent with those previously shown in zebrafish expressing CalipHluorin and FaNaC (Wang e al., 2014).

We conclude that unlike feed-forward glutamatergic transmission, which spills over to allow cross-talk between cone terminals, the proton change underlying HC feedback is compartmentalized to individual synaptic invaginations within a cone terminal. Provided the average distance between ribbon synapses and the diminished change in pH which we documented using both AMPApHluorin and synaptopHluorin the proton signal is consistent with private line communication.

The process of lateral inhibition and HC communication in the retina continues to pose scientific questions for research and debate. The models in this dissertation lay the foundation for additional experiments to investigate horizontal cell function and synaptic communication. While not explored in this dissertation, it would be interesting to see if hyperpolarization of HCs with the PSAM-GlyR would induce further alkalinization of the synaptic cleft or not. Future work might include preferential expression of FaNaC or PSAM-GlyR in specific HC types; *in vivo* Ca^{2+} imaging in the PSAM-GlyR or FaNaC fish crossed with HUC-GCaMP (presented in Chapter 2) while exposing them to different stimuli; or high throughput visual behavioral studies using zebrafish larva expressing the foreign channels. Our findings bring us a step closer to understanding the delicate relationship in the invaginated synapse formed between HCs and their surrounding bipolar cells and photoreceptors. This relationship proves to have spatially constrained communication via an unusual signal in the nervous system- protons, and is subject to a strict balance of HC membrane potential.

References

1. Baden T, Euler T, Weckström M, Lagnado L. Spikes and ribbon synapses in early vision. Trends Neurosci. 2013 Aug;36(8):480-8.
2. Baden T, Berens P, Franke K, Román Rosón M, Bethge M, Euler T. The functional diversity of retinal ganglion cells in the mouse. Nature. 2016 Jan 21;529(7586):345-50.
3. Barnes S, Grove JCR, McHugh CF, Hirano AA, Brecha NC. Horizontal Cell Feedback to Cone Photoreceptors in Mammalian Retina: Novel Insights From the GABA-pH Hybrid Model. Front Cell Neurosci. 2020 Nov 4;14:595064.
4. Euler T, Haverkamp S, Schubert T, Baden T. Retinal bipolar cells: elementary building blocks of vision. Nat Rev Neurosci. 2014 Aug;15(8):507-19.
5. Hoon M, Okawa H, Della Santina L, Wong RO. Functional architecture of the retina: development and disease. Prog Retin Eye Res. 2014 Sep;42:44-84.
6. Kamermans M, Fahrenfort I, Schultz K, Janssen-Bienhold U, Sjoerdsma T, Weiler R. Hemichannel-mediated inhibition in the outer retina. Science. 2001 May 11;292(5519):1178-80.
7. Kramer RH, Davenport CM. Lateral Inhibition in the Vertebrate Retina: The Case of the Missing Neurotransmitter. PLoS Biol. 2015 Dec 10;13(12):e1002322.
8. Kyrozis A, Reichling DB (1995) Perforated-patch recording with gramicidin avoids artifactual changes in intracellular chloride concentration. Journal of neuroscience methods 57:27- 35.
9. Masland RH. The fundamental plan of the retina. Nat Neurosci. 2001 Sep;4(9):877-86.
10. Miller RF, Dacheux RF (1983) Intracellular chloride in retinal neurons: measurement and meaning. Vision research 23:399-411.
11. Nelson R, Bender AM, Connaughton VP (2008) Transporter-mediated GABA responses in horizontal and bipolar cells of zebrafish retina. Visual neuroscience 25:155-165.
12. Wang TM, Holzhausen LC, Kramer RH. Imaging an optogenetic pH sensor reveals that protons mediate lateral inhibition in the retina. Nat Neurosci. 2014 Feb;17(2):262-8.
13. Wässle H. Parallel processing in the mammalian retina. Nat Rev Neurosci. 2004 Oct;5(10):747-57.

Bibliography

1. Nicholls, J. G., Martin, A. R., Fuchs, P. A., Brown, D. A., Diamond, M. E., & Weisblat, D. A. (2012). **From neuron to brain** (**5th ed**.). Sinauer Associates.
2. Luo, L. (2016). **Principles of neurobiology (1st ed.).** Garland Science.
3. Dowling, J. E. (1987). **The retina: An approachable part of the brain.** Cambridge, Mass: Belknap Press of Harvard University Press.
4. Rodieck, R. W. (1998). **The first steps in seeing.** Sinauer Associates.
5. Kandel ER, Schwartz JH, Jessell TM, Siegelbaum SA, Hudspeth AJ. **Principles of neural science (5th edition)**. Columbus, Ohio: McGraw-Hill Education; 2012.
6. Online Resource- Webvision by Helga Kolb- http://webvision.med.utah.edu/